Nuclear compression-mediated DNA damage drives ATR-dependent Lamin expression and mouse ESC differentiation

Tanusri Roy[1], Swetlana Ghosh[1], Niyati Piplani[1], Lakshmi Kavitha Sthanam[1], Niharika Tiwary[2], Sayak Dhar[1], W. Chingmei Wangsa Konyak[1], Santosh Surendra Panigrahi[1], Priya Singh[2], Divya Tej Sowpati[2], Sreelaja Nair[1], Sushil Kumar[1], P. Chandra Shekar[2], Shamik Sen[1*]

[1]Department of Biosciences & Bioengineering, IIT Bombay, Mumbai, India

[2]Centre for Cellular and Molecular Biology, Hyderabad, India

***Correspondence: shamiks@iitb.ac.in**

Abstract:

Embryonic stem cells (ESCs) which are susceptible to DNA damage depend on a robust and highly efficient DNA damage response (DDR) mechanism for their survival. However, the implications of physical force-mediated DNA damage on ESC fate remains unclear. We show that stiffness-dependent spreading of mouse ESCs (mESCs) induces DNA damage through nuclear compression, with DNA damage causing differentiation through early induction of Lamin A/C expression. Interestingly, differentiation is associated with rescue of DNA damage and activation of the DDR factor ATR. While ATR is typically known to play roles in DDR pathway, its role during stiffness-mediated nuclear compression and mESC differentiation is unknown. Nuclear enrichment of activated ATR on stiff substrates and reduction of Lamin A/C expression upon ATR inhibition suggests that mESC differentiation is driven by nuclear compression-mediated DNA damage and involves ATR-dependent modulation of Lamin A/C.

Keywords: ESCs, stiffness, Lamin A/C, ATR, nuclear compression, DNA damage, differentiation.

Introduction

Embryonic stem cells (ESCs) isolated from the inner cell mass of a late blastocyst of a developing embryo [1], serve as an important tool for studying pluripotency and development apart from stem cell-based therapies and genetic engineering [2]. Due to their high rate of proliferation and a shorter G1 phase [3,4], ESCs are particularly susceptible to DNA damage, and depend on a robust and highly efficient DNA damage response (DDR) mechanism to maintain their self-renewability and pluripotency [5]. ATM (Ataxia telangiectasia mutated) and ATR (ATM and Rad3-related) are key players entailed during DDR which are not only activated by DNA damage signals but also implicated in oxidative stresses [6,7], and metabolic processes [8,9]. While ATM senses DNA double stranded breaks (DSBs), ATR senses single stranded DNA that occurs due to replication stalling and DSB resection[10]. Single stranded DNA have been shown to activate ATR at DNA damage sites, which in turn activates Chk1[11]. However, DSBs with single stranded overhangs interfere with ATM activation and induce an ATM to ATR switch at these damage sites[12]. In addition, ATR also serves as a critical regulator during embryonic development, disruption of which can cause chromosomal fragmentation and lethality in early embryos[13] and premature age-related phenotypes in adult mice[14].

The dynamic stem cell microenvironment or the stem cell niche regulates stem cell fate through chemical (secretory) as well as physical cues necessary for survival and proliferation [15–20]. Force transmission to the nucleus through the linker of nucleoskeleton and cytoskeleton (LINC) complex modulates expression of mechanosensitive genes through chromatin reorganization [21–23] that directs stem cell differentiation [24] through extracellular matrix (ECM) stiffness [19] and topography [20]. Lamin A/C – a critical component of the LINC complex, not only plays an important role in maintenance of genome integrity [25–28] but also controls and contributes to nuclear mechanotransduction and stem cell fate determination [29–32]. Lamin A/C have been reported to maintain the naïve pluripotency of ESCs by being a critical regulator of chromatin organization while preventing aberrant cell fate decisions[33]. The nuclear lamina, majorly composed of lamins is subjected to dynamic assembly and disassembly by phosphorylation of Lamin A/C during mitosis [34]. Phosphorylation of Lamin A/C can also be induced by oxidative stress[35,36], heat shock response[37] as well as in response to low ECM stiffness[38]. Lamin A/C phosphorylation at Ser22 has been shown to cause its degradation[38] and nuclear softening which is crucial for protease independent migration of cancer cells [39].

Extreme nuclear deformation has been shown to cause nuclear membrane rupture leading to genomic instability [40–42] . Beyond their canonical DNA repair functions in somatic cells, recent studies have documented ATM/ATR activation in cells subjected to mechanical stresses [43–46]. While alterations in ATR can cause nuclear envelope breakdown and aberrant chromatin organization [43,44], loss in ATM triggers nuclear deformation and reduced Lamin A levels thus regulating nuclear stiffness and mechanics [47]. Given the association between ECM stiffness and chromosomal instability in mouse ESCs (mESCs) [48], in this study, we have probed the inter-relationships between ECM stiffness, DNA damage, DNA repair and mESC fate. By culturing mESCs on substrates of increasing stiffness, we show stiffness-dependent mechanoadaptation induces DNA damage through increased nuclear compression. This DNA damage in turn triggers stiffness dependent induction of Lamin A/C expression. While ATR plays a widespread role, we identify ATR as a regulator of Lamin A/C expression in mediating initiation of differentiation by obstructing Lamin A/C phosphorylation. Collectively, our study establishes stiffness-induced nuclear compression that mediates early ESC differentiation and ATR-dependent modulation of Lamin A/C expression.

Materials & Methods

Cell Culture & Reagents: E14 Tg2a mouse embryonic stem cells (mESCs) were cultured on 0.1% porcine gelatin (Sigma) coated dishes in presence of KO-DMEM (Gibco) and supplemented with 10% KO-Serum replacement (Gibco), 1X Glutamax (Gibco), 1X non-essential amino acids (NEAA) (Gibco) and 1X antibiotic-antimycotic (Gibco). These cells were supplemented with 10ng/ml leukemia inhibitory factor (LIF) and 0.1mM 2-mercaptoethanol (Gibco) to maintain pluripotency. Mouse embryonic fibroblasts (MEFs) were cultured in DMEM (Gibco) supplemented with 10% Fetal

Bovine Serum (FBS) of South American origin (Gibco) and 1X antibiotic-antimycotic (Gibco). Both mESCs and MEFs were maintained at 37^0C and 5% CO_2 concentration (NUAIRE incubator). For experiments, cells were dislodged with 1X TrypLE Express (Gibco) and seeded on glass or MEFDMs or polyacrylamide hydrogels (PA gels) coated with either 5µg/cm fibronectin (Merck) or 10µg/cm^2collagen-I (Sigma) without LIF. mESCs were treated with etoposide (ETO) (2µM, Sigma), Blebbistatin (Blebb) (5µM, Sigma), $MnCl_2$ (0.5 mM), N-acetyl cysteine (NAC) (5 mM, Sigma), Retinoic acid (RA) (1µM, Sigma), Ascorbic acid (AA) (50µM, Sigma), KU-55933 (10µM, Sigma) and VE-821 (5µM, Sigma) [49] for a period of 24 hours.

Fabrication of Polyacrylamide (PA) gels: PA hydrogels of varying stiffness of 0.6 kPa, 4 kPa and 33 kPa were fabricated by mixing varying ratios of 40% Acrylamide (Bio-Rad) and 2% Bis-Acrylamide (Bio-Rad) with milliQ water as described elsewhere [50,51]. Gels were polymerized on either 12mm,18mm or 60mm glass coverslips for immunostaining, comet assay and western blotting/flow cytometry experiments respectively. Gels were coated with either 10µg/cm^2 rat-tail collagen-I (Sigma) or 5µg/cm^2 human-plasma fibronectin (Merck) overnight in 4°C, post functionalization using Sulfo-SANPAH (Pierce).

Fabrication of MEF derived matrix (MEFDM): MEFDMs were generated by seeding WT MEFs (on 1% gelatin coated dishes (Porcine gelatin, Sigma) at a density of 4.6 x 10^5/cm^2 as described elsewhere in [48].

Immunostaining and Microscopy: For immunostaining, cells were fixed after 3 hours, 6 hours, 24 hours or 72 hours of culture using 4% PFA (Sigma) in PBS for 15 minutes, permeabilized with 0.1% TritonX-100 (Sigma) in PBS for 10 minutes, and then incubated with one or more primary antibodies overnight at 4°C post blocking with 5% FBS for 1 hr in room temperature. Primary antibodies used for immunostaining were against pMLC2-Ser19 (1:250, Cell Signaling Technologies), γ-H2AX (1:500, Cell signaling Technologies), Lamin A/C (1:400, Cell Signaling Technologies), Lamin B1 (1:500, Abcam), 53BP1 (1:2500, Invitrogen), pATM-Ser1981 (1:500, Invitrogen) and pATR-Thr1989 (1:500, Invitrogen). The following day, cells were washed with PBS and then incubated with one or more secondary antibodies at room temperature for 2 hours. Secondary antibodies used were Alexa-fluor 488 anti-mouse IgG (1:1000, Invitrogen), Alexa-fluor 555 anti-rabbit IgG (1:1000, Invitrogen). Cells were then stained with fluorescently labeled wheat-germ agglutinin (1:1000, Sigma) to stain cell surface and nuclei were labeled with DAPI (1:2000, Sigma). Cells were imaged at 120X magnification using either an inverted fluorescent microscope (Olympus, IX83) or at 63X magnification using Spinning Disc Confocal Microscope (Zeiss, CSU-X1) for greater resolution. Cell spreading area, DNA damage foci, mean intensities, nuclear enrichment and nuclear height were quantified using Fiji ImageJ software while nuclear volumes were quantified using Imaris X64 8.3.1. Stiffness and time-dependent Lamin A/C distributions were generated based by normalizing raw intensity values with the maximum value across all conditions and time-points. The normalized intensities (I_N) on a given stiffness gel (g) were categorized as low (Lo), Moderate (Mo) and High (Hi) based on the following criteria: Lo: $I_N \leq \mu_g - \sigma_g$, Mo: $\mu_g - \sigma_g < I_N \leq \mu_g + \sigma_g$, Hi: $I_N > \mu_g + \sigma_g$, where μ_g and σ_g correspond to the mean and the standard deviation of normalized intensity observed at the 3 hr time-point. The frequency curves were generated using Origin 2021. The percentage of Lo, Mo and Hi cells were calculated thereafter.

Comet Assay: To quantify the level of DNA damage in mESCs, alkaline and neutral comet assays were performed according to manufacturer's protocol (Trevigen). For this, mESCs were cultured on PA gels of varying stiffnesses. Post 24 hours, these cells were isolated from the gels using TrypLE Express (Gibco). 10 cells per ml were suspended in PBS and were mixed with 1% low melting agarose (GeneI) cooled to 37°C at a 1:10 v/v cell solution to agarose ratio. Approximately 50µl of the cell-agarose mixtures were evenly spread and incubated on comet slides (Trevigen) at 37°C for 5-10 minutes, and then transferred to 4°C in dark for 30 minutes until the agarose polymerized. The slides were then incubated overnight in ice cold lysis solution (Trevigen) at 4°C followed by alkaline denaturation for 1 hour to detect both single and double stranded DNA breaks. Electrophoresis was

carried out at 330 mA in the presence of ice-cold alkaline electrophoresis solution (pH>13) followed by 70% ethanol fixation for 5 minutes. To exclusively detect double stranded DNA breaks, neutral comet assay was performed by subjecting the cell-agarose mixture comet slides to run in presence of neutral electrophoresis solution (pH = 9) at 1V/cm, after overnight lysis at 4°C (same as alkaline assay). This was followed by a DNA precipitation step for 30 minutes and then fixation in 70% ethanol. Samples were stained with SYBR green dye (1:10,000, Invitrogen) diluted in 1X TE buffer and visualized under the microscope at 10X magnification. Comets were analyzed by feeding tif images into the OpenComet plugin in ImageJ Fiji software. Extent of DNA damage was quantified by comparison of the olive tail moment of mESCs on varying substrate stiffnesses.

AFM: Cell stiffness was measured using an Atomic Force Microscope (MFP3D, Asylum). Cells were probed with 10 kHz soft, pyramidal silicon nitride probes (Olympus) of nominal stiffness 20 pN/nm. The exact cantilever stiffness was determined using the thermal calibration method. Estimates of cell stiffness were obtained by fitting the first 500 nm of experimental force-indentation curves with Hertz model [52]. Similarly, the stiffness of gels was estimated by fitting the first 1000 nm of the experimental force-indentation curves as described elsewhere [51].

Western Blotting: mESC protein samples were isolated from mESC pellets using ice-cold RIPA buffer (Sigma) in the presence of freshly added 1% protease and phosphatase inhibitor cocktail (Invitrogen). Cell lysates were cleared by centrifugation at 12,000 rpm for 15 minutes at 4°C. Protein concentration was determined by Lowry method. 60 µg of total protein sample was loaded into each well and resolved by SDS-PAGE on gradient acrylamide-bisacrylamide gels (6% to 15%). Samples were transferred on to 0.2 µm PVDF membranes (Bio-Rad). Membranes were blocked with 5% BSA in TBST for 1 hour at RT and then incubated one or more of the following primary antibodies overnight at 4°C: Lamin A/C (1:1000, CST), pLamin A/C-Ser22 (1:1000, CST), Lamin B1 (1:1000, Abcam), γH2AX (1:1000, CST), H2AX (1:500, CST), pMLC2-Thr18/Ser19 (1:700, CST), MLC2 (1:700, Abcam), Oct3/4 (1:1000, Abcam and CST), Nanog (1:1000, CST), pATM-Ser1981 (1:1000, Invitrogen), pATR-Thr1989 (1:1000, Invitrogen), ATM (1:1000, CST), ATR (1:1000, CST), RAD51 (1:1000, Abcam), pCHK1-Ser345 (1:1000, CST), CHK1 (1:1000, CST), GATA4 (1:1000, Invitrogen), Brachyury (1:1000, Invitrogen), GATA3 (1:1000, Invitrogen), NeuN (1:1000, CST), pRPA2-Ser33 (1:700, Novus Biologicals) and GAPDH (1:1000, CST). The following day, after washing with TBST, membranes were incubated with HRP conjugated secondary antibody (1:10,000, Invitrogen) for 2 hours at RT. Subsequently, membranes were washed again with TBST and developed using ECL detection kits (Advansta), western BLoT Hyper HRP Substrate (Takara) and ultra-sensitive chemiluminescent substrate (Cynagen) for low abundant proteins. Blots were also subjected to stripping using western BLoT stripping buffer (Takara) according to manufacturer's protocol, followed by reprobing. Images were captured using a chemidoc imaging system (Bio-Rad).

RNA Sequencing (RNASeq) and heat map generation: Total RNA from bulk cells was isolated using TRIzol (Ambion) according to instructions from the manufacturer. The concentration and purity of samples was checked using the Nanodrop 2000 spectrophotometer. Ribo-Zero Plus stranded library preparation kit (Illumina) was used to generate libraries from a total of 1μg RNA for each sample. Library concentration was estimated using Qubit dsDNA High Sensitivity Assay Kit (Invitrogen). The libraries were sequenced on the Illumina NovaSeq 6000 platform to a depth of 50 million paired-end reads. The quality assessment of sequenced reads was evaluated using FASTQC (v0.12.0) followed by mapping them to the Mus_musculus.GRCm39.cdna reference cDNA transcriptome using Kallisto (v0.45.0) for estimating transcript abundance. Data annotation was carried out using AnnotationHub and genes exhibiting a Counts Per Million (CPM) value of less than 1 in at least three samples were excluded from further analysis. The resulting filtered count matrix was then normalized by Trimmed Mean of M-values (TMM) method using edgeR package, and was subsequently log2-transformed to mitigate data heteroskedasticity. Principal Component Analysis (PCA) was performed using the Scikit-learn library of python and a 3D PCA plot generated. Heatmaps were generated using Count matrix values followed by normalizing the data against +LIF control and then applying z-score

normalization across each row to get relative gene expression values. The representative matrices were sorted based on gene expression value of average of 72-hour samples.

Gene Ontology Analysis: Differential gene expression analysis conducted with the PyDESeq2 package identified upregulated and downregulated genes across stiffness conditions at 72 hours, using +LIF as a reference and applying a log2 fold change threshold of ≥ 1 and an adjusted p-value of ≤ 0.01. Following gene identification, gene ontology analysis via the gprofiler2 library was utilized to enrich transcription factor pathways. Subsequently, common transcription factor pathways upregulated across three stiffness conditions were identified. Prevalence of genes associated with endoderm, mesoderm, ectoderm and extraembryonic ectoderm lineage specification within each identified transcription factor pathway was quantified and sorted based on this occurrence frequency. The top 20 pathways were ranked based on their p-values and visually represented in a grouped bar chart format.

Flow cytometry: For cell-cycle analysis, mESCs were pelleted down using TrypLE Express (Gibco) and fixed using 0.25% PFA for 15 minutes on ice followed by permeabilization with 70% methanol in 4°C for at least 1 hour. Cell pellets were washed with PBS to remove residual methanol and then 50µg/ml Propidium Iodide (Himedia) was added to each condition before acquisition for cell cycle measurements on BD FACS Aria Fusion. Gating was done with respect to pluripotent mESCs using FlowJo software. For apoptosis assay, mESC pellets were incubated with FITC conjugated Annexin V and Propidium Iodide in 1X binding buffer as per manufacturer's protocol (BD Pharmingen). 10,000 events were acquired per sample. Gating was done with respect to unstained control using FlowJo software.

Pharmacological inhibition assays using zebrafish embryos: *Tg(cmlc2):mCherry* embryos were raised in embryo medium at 28°C till 24 hours post fertilization (hpf). At 24 hpf, embryo medium was replaced with embryo medium containing 10µM KU55933 or 10µM VE821. Embryos were kept in the inhibitors for 24 hours at 28°C. The next day, the medium was replaced with fresh embryo medium without inhibitors and embryos were left to grow for another day. Heart phenotypes were quantitated and imaged at 48 hpf (24 hours of exposure to inhibitor) and at 72 hpf (24 hours of exposure to inhibitor, followed by 24 hours of recovery). Live images were obtained using Olympus MVX10 and processed using CellSens and ImageJ softwares.

Statistical Analysis: For statistical analysis, raw data were processed in Origin 2021. The normality of the data was first checked using the Kolmogorov-Smirnov normality test. Based on these results, either parametric or nonparametric tests were subsequently performed. Statistical significance was assessed using unpaired t-tests for comparing two parametric datasets. One-way or two-way ANOVA tests were performed for parametric datasets with multiple conditions, followed by Tukey's post-hoc test to compare the means. For multiple non-parametric datasets, Kruskal-Wallis ANOVA followed by Dunn's post-hoc test while Mann-Whitney test for comparing means between two non-parametric datasets were performed. $p < 0.05$ being considered as statistically significant.

Results

Stiffness-mediated mechanoadaptation is associated with DNA damage in mESCs

Long-term culture of mESCs on stiff gelatin-coated coverslips have been shown to accumulate greater aneuploidy compared to that on mouse embryonic fibroblast (MEF) derived matrices, which are much softer [48]. To probe the link between stiffness-mediated mechanoadaptation and genomic integrity, we cultured mESCs on collagen (Col) and fibronectin (FN) coated 0.6 kPa, 4 kPa and 33 kPa PA gels that span a physiologically relevant stiffness range (Fig. S 1A). As mESCs exhibited greater spreading and focal adhesion intensities on FN coated gels compared to that on Col coated gels, indicative of a more robust mechanoadaptation response on FN coated gels (Fig. S 1A, B), all subsequent experiments were performed on FN coated substrates up to 72 hrs in culture. While mESCs spread minimally on the softest 0.6 kPa gels, spreading increased substantially on the 4 and 33 kPa gels (Fig. 1Ai, ii).

Increased spreading on 4 and 33 kPa gels was associated with increased cytoskeletal organization as assessed by active actomyosin contractility (phosphorylated myosin light chain, pMLC) (Fig. 1Bi, ii, Fig. S 1C) and cortical stiffness (Fig. 1 Ci, ii). Interestingly stiffness-mediated mechanoadaptation was associated with stiffness-dependent increase in the extent of DNA damage assessed by counting the number of γH2AX foci in individual cells (Fig. 1 Di, ii) and total protein levels assessed using westerns (Fig. 1 Diii). Since γH2AX marks both single and double strand breaks[53–55], to determine the relative proportion of single and double strand breaks across different stiffnesses, we performed alkaline comet assay which detects both type of breaks, and neutral comet assay which detects double strand breaks (Fig. 1 Ei, ii). Stiffness-dependent increase in olive tail moments in both the assays suggests the presence of both single and double strand breaks. However, greater stiffness dependent change in olive tail moments in alkaline comet assay compared to neutral comet assay indicates higher proportion of single strand breaks with increase in substrate stiffness. Together, these results establish a direct relationship between stiffness-dependent mechanoadaptation and DNA damage in mESCs.

DNA damage is induced by mechanoadaptation-mediated nuclear compression

To test if stiffness-induced DNA damage was ROS dependent, DNA damage was assessed by quantifying γH2AX foci in cells cultured in the presence and absence of the ROS scavenger N-acetyl cysteine (NAC). Insensitivity of DNA damage to NAC suggests that mechanoadaptation-mediated DNA damage in mESCs is ROS independent (Fig. 2 Ai, ii). Contractility-mediated nuclear compression has been shown to induce nuclear envelope rupture and DNA damage in cancer cells cultured on rigid glass coverslips [40]. To check the link between DNA damage and nuclear compression, we captured transverse sections of Lamin B1-stained nuclei of mESCs cultured on different gels and quantified nuclear height. Increased DNA damage on stiffer substrates was associated with increased nuclear compression observed as early as 3 hrs (Fig. 2 Bi, ii). In comparison, nuclear volume increased marginally with time but remained unchanged across different gels (Fig. 2 Biii).

Based on these results, we propose that increased spreading and cytoskeletal organization on stiffer substrates induces DNA damage by nuclear compression. To test this, the extent of nuclear compression was perturbed by modulating cell spreading, and its impact on DNA damage assessed. While cells were treated with $MnCl_2$ on 0.6 kPa gels to increase cell spreading via increased integrin association [56–58], on 33 kPa gels, cells were treated with the contractility inhibitor blebbistatin (Blebb) (Fig. 2 Ci). On 0.6 kPa gels, $MnCl_2$ treatment led to increased spreading (Fig. 2 Cii, iii), decreased nuclear height (Fig. 2 Cii, iv), increased γH2AX foci (Fig. 2 Di, ii) and increase in olive tail moment assayed using alkaline comet (Fig. 2 Fi, ii). Conversely, on the stiff 33 kPa gels, treatment with Blebb led to decreased cell spreading (Fig. 2 Cii, iii), increase in nuclear height (Fig. 2 Cii, iv), reduction in the extent of DNA damage (Fig. 2 Di, ii), and decrease in olive tail moment (Fig. 2 Fi, ii). Western blotting of total cell lysates revealed increased pMLC and γH2AX levels in $MnCl_2$-treated cells, and the opposite in Blebb-treated cells (Fig. 2 E). Collectively, these results demonstrate that mechanoadaptation-mediated nuclear compression induces DNA damage in mESCs.

DNA damage induces loss of pluripotency and Lamin A/C expression

Lamin A/C is an integral part of the nuclear membrane that plays a key role in nuclear mechanics as well as in genome protection. ECM stiffness has been shown to drive differentiation of mesenchymal stem cells (MSCs) with induction of Lamin A/C expression [19,20,32] and affect ESC differentiation [59,60]. However, the importance of stiffness-induced DNA damage in this context remains unclear. Interestingly, increase in Lamin A/C levels on 4 kPa and 33 kPa gels and drop in pluripotency markers Oct3/4 and Nanog suggests that DNA damage may drive early differentiation (Fig. 3 Ai, ii). To test this, experiments were performed wherein DNA damage was induced with low doses of the topoisomerase II inhibitor – etoposide (ETO) and its impact on pluripotency and Lamin A/C expression assessed on the softest 0.6 kPa gels, where mechanoadaptation and DNA damage were lowest (Fig. 3 Bi). Remarkably, ETO treatment led to robust increase in Lamin A/C levels with corresponding loss in Oct3/4 and Nanog expression, suggesting that low doses of DNA damage also induce loss in pluripotency and induction of Lamin A/C expression (Fig. 3 Bii, Biii). To understand

the temporal kinetics of Lamin A/C induction triggered by DNA damage, mESCs cultured on 0.6 kPa gels for 6 hrs (to allow for initial attachment) were incubated with 2 μM of ETO, and Lamin A/C levels tracked upto 3 hrs post treatment (Fig. 3 Ci). Both DNA damage and Lamin A/C remained unchanged upto 2 hrs of ETO treatment but increased significantly at the 3 hr time-point (Fig. 3 Cii, iii). The same held true for pluripotency markers, Oct3/4 and Nanog, with significant loss in pluripotency at the 3 hr timepoint.

To assess if chemical factor induced differentiation also involves DNA damage, mESCs cultured on the softest 0.6 kPa gels in the presence of the neuronal differentiation factor retinoic acid (RA) and the osteogenic differentiation factor ascorbic acid (AA) were probed for DNA damage and Lamin A/C levels at 3 and 24 hr time-points (Fig. 3 Di). Both RA and AA treatments led to increased levels of the neuronal marker, β-III tubulin at the 24 hr time-point (Fig. S 1Di, ii). Strikingly, both RA and AA treatment led to increase in γH2AX and Lamin A/C levels, and loss in Oct3/4 levels at the early 3 hr time-point (Fig. 3 Dii, iii). Though Nanog was unchanged at the 3 hr time-point, near complete loss in its expression was observed at 24 hrs indicative of differentiation. Surprisingly, at this timepoint both γH2AX and Lamin A/C levels dropped to baseline levels. In comparison, no change in Lamin B1 levels was observed.

To further probe the occurrence of DNA damage during mESC differentiation on more *in-vivo* mimetic conditions, we cultured mESCs on mouse embryonic fibroblast (MEF) derived matrices (MEFDMs) which induce mESC differentiation [61] (Fig. S 2 Ai, ii). In comparison to mESCs cultured on gelatin-coated glass coverslips in the absence of LIF (serving as controls, CTL), in mESCs cultured on MEFDMs for 24 hrs, increase in γH2AX, loss in Oct3/4 levels and induction of Lamin A/C was observed (Fig. S 2 Bi-iii) when normalized to GAPDH levels (which remained lower for mESCs on MEFDM). While Nanog levels remained unchanged, surprisingly, loss in Lamin B1 was observed. In MEFs which possess high levels of Lamin A/C, no DNA damage was observed. Collectively, our results suggest DNA damage induces loss of pluripotency and Lamin A/C expression.

Temporal loss of pluripotency is associated with mechanoadaptation mediated differentiation in mESCs

Stimulation by differentiation factors cause pluripotent mESCs to differentiate into either endoderm, ectoderm or mesoderm layers. To probe how mechanoadaptation mediated loss in pluripotency and induction of Lamin A/C expression influences mESC fate, these cells were cultured up to 72 hrs on the PA gels and RNA sequencing (RNAseq) performed at 3, 6, 24 and 72 hr time-points. Principal Component Analysis (PCA) plot shows a clear time dependent clustering of mESCs, with no prominent stiffness dependence (Fig. 4 A). Though DNA damage and Lamin A/C induction was also seen in ETO treated cells, this point did not co-cluster with any of the other time-points. Compared to pluripotent controls (+LIF), temporal RNAseq profiling revealed stemness genes including *Pou5f1* [62,63], *Sox2* [64], *Nanog* [65,66] and *Klf4* [67] were maintained till 6 hrs, but were lost completely at the 24 hr time-point (Fig. 4 B). Similar trend was also observed in western blots of Oct3/4 and Nanog (Fig. 4 Ci, ii). Concomitant with loss in pluripotency, several known lineage-specific markers were upregulated at the 72 hr time point. These included endoderm markers such as *Cldn6* [68,69], *Gata4* [70], *Sox17* [71] and *Foxa2* [72,73], mesoderm markers such as *Tbx6* [74,75], *Twist1*[76–78] and *Snai1* [79,80], and ectoderm markers such as *Nes* [81] and *RunX2* [82] (Fig. 4 B, Fig. S 3 A). Intriguingly, expression of extraembryonic ectodermal markers such as *Krt8* [83], *Wnt7b* [84] and *Gata3* [85] was also observed. While these results are indicative of heterogeneous differentiation, quantification of the average Z-score values across the three stiffnesses revealed most prominent induction of mesoderm lineage (0.4), and weaker induction of endoderm (0.14) and ectoderm (0.1) lineages, indicating a shift towards mesodermal lineage. Protein level expression of one marker from each lineage – Gata4 for endoderm, Brachyury (T) for mesoderm and NeuN for ectoderm – showed similar trend with RNAseq profiles (Fig. S 4 Ai, ii). In addition, gene ontology analysis revealed lineage specification is mediated by activation of several common transcription factors such as *Zf5*, *E2F*, *SP3*, *Kaiso*, *Pax4*, *Foxn1* (Fig. S 3 B).

Temporal RNAseq profiling of Lamin genes across the 4 time-points revealed an increase in *Lmna* gene but drop in *Lmnb1* and *Lmnb2* genes as expected in differentiating stem cells (Fig. 4 Di). Although Lamin A/C is known to enhance differentiation of MSCs [32], surprisingly however, protein level analysis shows a gradual decline in both Lamin A/C and Lamin B1 across all the gels, prominently at the 72 hr time-point (Fig. 4 Dii, iii) with considerable heterogeneity in Lamin A/C expression in each condition (Fig. 4 Ei, Red arrowhead: Lamin A/C high; Yellow arrowhead: Lamin A/C low). Lamin A/C intensity distribution revealed an increase in the fraction of Lamin A/C low (Lo) cells at 72 hrs across all the gels (Fig. 4 Eii, iii), with ~30%, 50% and 40% Lamin A/C low cells at 72 hrs on 0.6 kPa, 4 kPa and 33 kPa gels respectively (Fig. 4 Eiii). However, long term culture of mESCs upto 7 days on the stiff 33 kPa gels, exhibited a recovery of Lamin A/C levels after its initial decline at 72 hrs (3 days) (Fig. S 4B), consistent with previous findings that shows that Lamin A/C loss primes mESCs towards cardiac-specific gene expression [31,33]. Since, genome integrity is associated with an intact nuclear envelope devoid of blebs and rupture [42,86], evaluation of the nuclear lamina using confocal image of Lamin B1, revealed no detectable nuclear blebbing until the 24 hr timepoint on the stiff gels. However, mESCs were seen to exhibit nuclear wrinkling at 72 hrs of culture on these gels (Fig. S 4C).

Since, *LMNA* deficient embryonic hearts have been shown to exhibit cell cycle perturbations during DNA damage [87], we next went on to evaluate the cell cycle distribution of mESCs on the PA gels at different time-points. Quantitative analysis showed that sub-G1 phase significantly increased with time – from <20% cells in +LIF mESCs to ~40% cells at 72 hrs and ~80% upon ETO treatment (Fig. S 5 Ai, ii). The Sub-G1 cells at 72 hrs may correspond to that of low Lamin A/C expressing mESCs at the same time-point on 33 kPa gels (Fig. 4 Ei-iii), suggesting that transient Lamin A/C loss affects mESC cell cycle distribution on PA gels. Furthermore, quantification of cell survival using Annexin V-PI staining revealed ~60% live mESCs at 72 hr time-points on all the gels compared to ~85% live cells in presence of LIF (Fig. S 5 Bi, ii). While temporal RNASeq profiling revealed activation of few apoptosis genes (*Casp8, Casp6, Casp7*) at 72 hrs time-point (Fig. S 5 C), Annexin-PI staining shows no significant increase in apoptotic cells but % necrotic cells were dramatically increased at 72 hr time-point and upon ETO treatment (Fig. S 5 Bi, ii).

Since embryogenesis is mediated by cell-matrix adhesions and mechanical forces [88] that control complex mechano-signaling cascades via integrins [89], we examined the temporal profile of several genes involved in mechanoadaptation. RNAseq profiles show clear upregulation of several such genes at 72 hrs such as integrin subunits – *ItgaV, Itga3, Itga11, Itgb1, Itgb3, Itgb5, Itgb8*, integrin like kinase (*Ilk*), genes involved in integrin mediated cell adhesion – *Tln1, Vcl, Gsn, Tsn2, Parva, Parvb, Acta1, Acta2, Actg1*, myosin genes – *Mylk, Myl6, Myl9, Myl12a, Myl12b*, along with *Cdh1* and *Cdh2* (Fig. S 4 D). Few LINC complex genes were also upregulated at 72 hrs such as *Sun2, Syne2* and *Lmna* (Fig. S 4 D), thus implicating an integrin dependent mechanoadaptation response that mediates mESC differentiation at 72 hrs. Together, these results suggest that loss in pluripotency in mESCs is associated with transient loss of Lamin A/C protein expression leading to early differentiation (72 hrs) into all three germ layers (with a prominent shift towards mesodermal lineage) through activation of mechano-signaling pathways.

mESC differentiation is associated with ATR activation

While mESCs have a robust DNA damage response (DDR) mechanism to counter intrinsic and extrinsic assaults to the genome, compared to their differentiated counterparts [90], accumulation of DNA damage can cause apoptosis and differentiation to eradicate them from the stem cell pool [91–93]. We propose that differentiation is triggered via activation of DDR pathways and DNA repair. Consistent with this notion, temporal immunostaining and quantification of γH2AX foci on mESCs displays a steady level upto 24 hrs and then a sharp decline at the 72 hr time-point (Fig. 5 Ai, ii). Similarly, 53BP1 quantification shows a significant increase at 6 hrs which then notably diminished at the 72 hr time-point (Fig. 5 Bi, ii), indicative of a temporal resolution of DNA damage. To further confirm our observations, immunoblotting of mESCs also revealed a significant drop in γH2AX as well as pRPA2 (Single strand break marker) levels at the 72 hr time-point. (Fig. 5 C, Fig. S 6 Ai, ii).

RNAseq profiles of early responders of DNA damage revealed upregulation of *ATR* and *RAD50*, downregulation of *ATM, Mre11a, MDC1, Trp53bp1, RPA1, RPA2, Atrip*, and upregulation of downstream DNA repair genes including *Brca2* and *Rbbp8* at 72 hr time-point (Fig. 5 D). These observations motivated us to investigate the functional roles of ATM and ATR during stiffness mediated mechanoadaptation in regulating lamin levels. No phosphorylated ATM (pATM, Ser1981) bands were detected on 33 kPa gels across the different time-points, notwithstanding the fact that ATM levels remained unchanged across these conditions when compared to +LIF condition (Fig. 5 Ei, Fig. S 6 B). However, pATM was detected in immunostained images of mESCs cultured on 33 kPa gels (Fig. 5 Fi), and exhibited uniform spatial distribution (Fig. 5 Fii, iii). In contrast to ATM, phosphorylated ATR (pATR, Thr1989) was detected from 3 hr onwards (Fig. 5 Ei, ii Fig. S 6 B). Furthermore, quantification of nuclear to cytosolic (N/C) ratio revealed increased nuclear localization of pATR across all time-points (Fig. 5 Fiii) with greater nuclear enrichment on the stiffer 33 kPa gels (Fig. S 6 C). Near complete loss in RAD51 levels at the 72 hr time-point (Fig. 5 D, Ei, ii) may correspond to resolution of DNA damage and mESC differentiation (Fig. 5 A, B and C). Taken together, these results suggest that DNA damage-induced differentiation is associated with ATR mediated DDR activation followed by DNA repair.

Furthermore, since RNAseq analysis of mESCs revealed an upregulation of mesodermal genes, we analyzed the effect of inhibiting DNA repair on development of the heart, a mesodermal organ, which is also mechanically active during its formation. The zebrafish heart forms as a tube and develops into a two-chambered contractile organ by 24 hours post fertilization (hpf). The heart then undergoes morphogenetic movements resulting in a left-ward ventricle and right-ward atrium and chamber ballooning by ~72 hpf [94]. Zebrafish embryos exposed to ATM and ATR inhibitors (KU55933 and VE821 respectively) for 24 hours showed mild body curvature defects at 48 hpf (Fig. S 6 Di, ii, n=71 for KU and n=73 embryos for VE) and defects in chamber size and ballooning (Fig. S 6 Dii). Following 24 hours exposure to inhibitors, larvae were allowed to recover in inhibitor-free medium for another 24 hours. However, the defects in heart morphogenesis worsened by 72 hpf, wherein the ventricle and atrium failed to attain their characteristic ballooning and left-right positioning in the larvae (Fig. S 6 Diii, n=35 for KU and n=44 embryos for VE, Supp. movies S1 to S3). Interestingly, in several embryos cardiac contractility was absent at 72 hpf (7/35 for KU and 2/44 for VE). These results suggest that ATM and ATR function is required for normal morphogenesis of the developing zebrafish heart and inhibition of ATM/ATR during cardiac morphogenesis causes inability of embryos to recover from the damage.

ATR regulates mESC survival and differentiation by temporal modulation of Lamin A/C

Physical properties of the nucleus are dictated by Lamin A/C levels with its phosphorylation a Ser22 leading to its degradation [32,38], and inducing nuclear softening[39]. While DNA damage induces Lamin A/C expression at early time-points, Lamin A/C was lost at the 72 hr time-point (Fig. 4 D, E). To probe how DNA damage, DDR response and Lamin A/C degradation are temporally correlated, we tracked γH2AX/H2Ax, pATR/ATR, pCHK1/CHK1, and pLamin A/C (S22)/Lamin A/C over a period of 1 week on 33 kPa gels (Fig. 6 Ai, ii). Similar to ETO treatment (Fig. 3 C), temporal kinetics revealed γH2AX activation at 1 hr precedes Lamin A/C induction at the 3 hr time-point. Lamin A/C induction was associated with CHK1 activation. Subsequent drop in Lamin A/C correlated with increase in pLamin A/C, while pATR levels remained constant. However, increase in pATR after 72 hr was associated with rescue in Lamin A/C levels and concomitant reduction in pLamin A/C levels.

Since both ATM and ATR have been linked to regulation of nuclear envelope integrity and lamin levels [43,47,95], we assessed the role of ATM and ATR in regulating Lamin A/C levels. In mESCs cultured in the presence of ETO, though both ATM and ATR were activated, ATR/CHK1 activation was more prominent and correlated with drop in pLamin A/C and increase in Lamin A/C levels (Fig. 6 Bi-iii). To test if ATR regulates Lamin A/C by modulating Lamin A/C phosphorylation, we performed experiments with KU and VE on 33 kPa gels (Fig. 6 Ci). Both inhibitors led to drop in γH2AX foci counts and levels (Fig. 6 Cii-iv). However, only ATR inhibition led to increase in pLamin A/C and decrease in Lamin A/C levels, suggesting that ATR stabilizes Lamin A/C by

preventing this phosphorylation (Fig. 6 Cii, D). Even Lamin B1 levels were reduced upon ATR inhibition.

Finally, to investigate the role of ATR activity in mESC cell cycle distribution, viability and differentiation, we analyzed the percentage cell cycle distribution and observed increased SubG1 cells upon VE treatment indicative of a perturbed cell cycle pattern that corresponds to significant reduction in cell viability (Fig. S 7 A, B). Furthermore, assessment of mESC pluripotency and differentiation revealed prominent reduction in Oct3/4 and Nanog levels upon ATR inhibition coupled with significant increase in the extraembryonic ectoderm marker GATA3 and decrease in the mesoderm marker Brachyury (T) (Fig. 6 E). In comparison, GATA4 and NeuN remained unchanged. Taken together, in addition to its role in DDR, our observations suggest that ATR regulates mESC survival and differentiation by modulating Lamin A/C in a temporal manner.

Discussion

Genome integrity has been associated with transmission of physical forces to the nucleus leading to nuclear envelope deformation, blebbing and rupture in cancer cells [40,42]. Lamin A/C is a crucial component of the nuclear envelope with Lamin A/C deficiency causing laminopathies [96], increased DNA damage [28,97,98], and defective mechanotransduction [30]. Additionally, drug induced DNA damage alters chromatin condensation state resulting in alterations in the biomechanical properties of the nucleus through DDR signaling, thus establishing a link between genome integrity, DNA damage signaling, chromatin condensation and nuclear mechanics [99]. Here, using FN coated PA gels of varying stiffness, we report stiffer matrices trigger greater DNA damage in mESCs through increased nuclear compression. We show that DNA damage brings about loss in pluripotency and Lamin A/C induction at early time-points, thus functioning as a mediator of early differentiation. Differentiation of mESCs at the 72 hr time-point was associated with early induction of DNA damage response factors (γH2AX, 53BP1 and pRPA2) and downstream DNA repair factors (RAD51). Of the two DNA damage response (DDR) factors ATM and ATR, we establish a role for ATR in modulating and stabilizing Lamin A/C expression by inhibiting its phosphorylation. Collectively, our results demonstrate how stiffness-dependent DNA damage drives differentiation through ATR-dependent Lamin regulation (Fig. 7).

ATR is activated by single stranded breaks (SSBs) during replication stress that arise due to stalled replication forks and at resected DSBs [11,100]. As part of the DDR pathway, ATR directly phosphorylates the checkpoint kinase, CHK1 at Ser-345 [101]. High proliferative capacity of mouse ESCs have been previously shown to contribute to increased accumulation of SSBs and involves ATR mediated activation of H2AX and CHK1 [53,54]. To assess the nature of DNA damage induced by stiffness, we performed alkaline comet assay which detects both SSBs and DSBs, and neutral comet assay which exclusively detects DSBs. Though both SSBs and DSBs were observed, significantly higher stiffness-dependent increase in olive tail moment of alkaline comets compared to neutral comets suggests that stiffness primarily induces SSBs in mESCs and is correlated with ATR activation. While SSBs are most commonly induced by oxidative stresses[102–104] , insensitivity of γH2AX to the ROS inhibitor NAC indicates that stiffness—induced DNA damage is ROS independent.

Stem cell maintenance and differentiation are regulated by several components of the stem cell niche. Cell-ECM interactions are known to regulate stem cell self-renewability and differentiation[105]. While collagen-I (Col-I) has been reported to maintain mESC self-renewability[106], fibronectin (FN) has been associated with self-renewability as well as differentiation[107–109]. MEFDMs of different composition, organization and stiffness have been shown to induce distinct mESC germ layer commitment [61]. In addition to its association with stem cell self-renewability and lineage commitment[19,32,60,110], matrix stiffness has also been implicated in regulating genomic integrity (ploidy) of mESCs [48]. Our findings establish a direct link between stiffness mediated mechanoadaptation and DNA damage in mESCs on FN coated PA gels. While MSCs and cancer cells undergo nuclear compression, DNA damage and

nuclear envelop rupture during confined migration[40,42,111,112]; we show for the first time that DNA damage in mESCs is attributed to stiffness-dependent nuclear compression and subsequent nuclear wrinkling. Stiffness-dependent differences in nuclear compression observed as early as 3 hrs can be attributed to stiffness-dependent alterations in actomyosin contractility as Blebb treatment on 33 kPa reduced nuclear compression and DNA damage, and $MnCl_2$ treatment on 0.6 kPa gels led to increased nuclear compression and DNA damage. Our results are consistent with earlier reports which showed suppression of DNA damage in embryonic hearts by lowering of contractility mediated nuclear deformation[87].

Literature reports have documented opposite effects of DNA damage in inducing differentiation. While genotoxic DNA damaging agents have been shown to disrupt myogenic differentiation[113], physiological DNA damage induced by caspase 3 has been shown to promote differentiation[114]. Moreover, confined migration has been reported to cause impaired cell cycle and delayed differentiation in myoblasts[115]. LIF maintains *in-vitro* mESC self-renewability through the STAT3 pathway [116], and has been implicated as a mechano-inhibitor [48]. In mESCs, LIF withdrawal triggers an exit from pluripotency and induction of apoptosis [117]. However, mESCs on soft substrates maintain pluripotency even in absence of LIF by downregulation of traction forces [60]. Using RNA sequencing analysis and western blotting we show temporal downregulation of most stemness markers accompanied by upregulation of differentiation genes involved in germ layer commitment, in the absence of LIF. In line with previous observations [117,118], temporal cell survivability assay on mESCs show ~ 40% dead cells at 72 hr time-point. These observations suggests that a proportion of mESCs undergo cell death which could be triggered due to LIF withdrawal for longer duration. Since we also observed time dependent impairment of cell cycle and loss in mESC survivability with ~60% Sub-G1 cells, the cells undergoing mixed lineage differentiation at the 72 hr time-point likely correspond to the surviving cells where DNA damage in resolved. Consistent with this, expression of the DNA repair protein RAD51 reduced at 72 hrs.

While conflicting reports exist on Lamin A/C expression in mESCs[119,120], our results reveal non-monotonic alterations in Lamin A/C levels during differentiation. Basal levels of Lamin A/C observed in +LIF conditions is consistent with its role in maintenance of naïve pluripotency and prevention of premature differentiation[33]. By temporally profiling γH2AX and Lamin A/C levels, that stiffness-induced DNA damage precedes induction of Lamin A/C. Induction of Lamin A/C observed at early time-points may contribute to DNA repair in multiple ways. First, stable Lamin A/C localization at the nuclear lamina confers mechano-protection to the genome [87]. Second, by anchoring damage sites via 53BP1, it can mediate efficient repair[28,121,122] as evident from ATR/CHK1 activation. Gradual loss of Lamin A/C from 24 hr onwards can be attributed to increased Lamin A/C phosphorylation and degradation[38] leading to nuclear softening[39]. Given the heterogeneity in Lamin A/C expression, and close correlation between the proportion of low Lamin A/C expressing cells and the proportion of dead cells, it is likely that low Lamin A/C cells may correspond to the genetically defective cells that are eliminated from the stem cell pool during differentiation [123,124], with restoration of Lamin A/C at Day 7 corresponding to differentiated cells. Thus, Lamin A/C plays a temporally differential role during stiffness induced mESC differentiation with induction at early timepoints protecting the genome, and loss at intermediate timepoints initiating differentiation.

Apart from the canonical DNA damage response exhibited by ATM and ATR, these factors have been extensively linked to nuclear envelope integrity, regulation of lamins and mechanosensitivity during cancer migration and invasion [43–47,95]. While ATM has been claimed to be activated by cell stretching[46], ATR is activated by nuclear compression during interstitial migration[43]. Another study has shown the role of ATR in Lamin A/C phosphorylation at Ser 282 in response to DNA damage, leading to alterations in nucleo-cytoskeletal and chromatin organization [95]. Here, we show that pATM is uniformly present in nucleus and cytosol, but pATR selectively localizes to the nucleus on stiff gels. Temporal analysis of our study suggests that although pATR levels remain unchanged till 72 hr timepoint, constitutive nuclear localization and pCHK1 activation synchronous with Lamin A/C levels is indicative of a connection between ATR activation and Lamin A/C modulation. Since ATR

stabilizes Lamin A/C by inhibiting its phosphorylation, we posit that differential role of Lamin A/C during differentiation is regulated by ATR/CHK1.

ATR is known to be developmentally essential[14] and has been stated to mediate fate decisions in ESCs during replication stress[125]. Our experiments in zebrafish embryos also show that ATM and ATR function is required for normal morphogenesis of the mechanically contractile zebrafish heart during critical stages of cardiac development. The changes in shape and size of the heart together with the heart beat defects indicate that cell fate specification and cell differentiation processes may be affected. Interestingly, substantial increase in pATR levels on Day 7, in line with Lamin A/C restoration is indicative of its role in initiation of stiffness dependent mESC differentiation. Although inhibition of ATR activity does not significantly change; levels of GATA4, Brachyury and NeuN, increase in levels of GATA3, the extraembryonic ectoderm was observed. This points towards the idea that the ATR/CHK activity could be responsible for maintaining mesodermal lineage specification during stiffness induced mechanoadaptation, while its suppression drives extraembryonic ectodermal lineage specification as seen from our RNA seq data and western blots at 72 hr time point. Taken together, our results indicate a novel role of matrix stiffness induced nuclear compression that triggers DNA damage in activating ATR within the nucleus, and driving ESC differentiation through modulation of Lamin A/C.

In conclusion, our results illustrate the role of matrix stiffness in mediating nuclear compression in mESCs leading to DNA damage. Our results also show that such DNA damage not only drives early differentiation and Lamin A/C induction but also activates and localizes ATR to the nucleus, indicative of the role of ATR in modulating lamin expression in mESCs during mechanoadaptation.

Acknowledgements

Authors acknowledge financial support from the Department of Biotechnology (Govt. of India) (Grant # BT/PR34522/MED/31/417/2019) and intramural funds provided by IIT Bombay. TR was supported by a CSIR fellowship (Grant # 09/087(0927)/2017-EMR-I) (Govt. of India). Authors would also like to thank IRCC, IIT Bombay for providing Bio-AFM and confocal microscopy facilities, and DST FIST sponsored FACS facility. Authors are deeply grateful to Prof. Anirban Banerjee and Prof. Santanu Kumar Ghosh, Department of Biosciences and Bioengineering, IIT Bombay for their critical inputs and suggestions.

Author contributions

Conceptualization: T.R., S.K., S.N., C.S.P., S.S.; Methodology: T.R., S.G., N.P., S.D., N.T., C.W.K., S.S.P., P.S., S.G., L.K.S., D.T.S., S.N., C.S.P., S.K, S.S.; Software: T.R., S.D., N.T., C.W.K., P.S., D.T.S., C.S.P., S.N., S.K., S.S.; Validation: S.S.; Formal analysis: T.R., S.D., S.G., N.T., C.S.P., S.K., S.S.; Investigation: T.R., S.K., S.N., S.S.; Resources: S.S.; Data curation: T.R., S.G., N.P., S.D., N.T.; S.S.P.; C.S.P.; S.K., S.S.; Writing - original draft: T.R., S.S.; Writing - review & editing: T.R., N.P., S.D., C.W.K., N.T., C.S.P., S.N, S.K., S.S.; Visualization: T.R., S.S.; Supervision: S.S.; Project administration: S.S.; Funding acquisition: S.S.

Declaration of Interests

The authors declare no competing interests.

References

1. Martin, G.R. (1981). Isolation of a pluripotent cell line from early mouse embryos cultured in medium conditioned by teratocarcinoma stem cells. Proc Natl Acad Sci U S A *78*. https://doi.org/10.1073/pnas.78.12.7634.

2. Doss, M.X., Koehler, C.I., Gissel, C., Hescheler, J., and Sachinidis, A. (2004). Embryonic stem cells: A promising tool for cell replacement therapy. Preprint at Journal of Cellular and Molecular Medicine, https://doi.org/10.1111/j.1582-4934.2004.tb00471.x https://doi.org/10.1111/j.1582-4934.2004.tb00471.x.

3. Kapinas, K., Grandy, R., Ghule, P., Medina, R., Becker, K., Pardee, A., Zaidi, S.K., Lian, J., Stein, J., van Wijnen, A., et al. (2013). The abbreviated pluripotent cell cycle. Preprint, https://doi.org/10.1002/jcp.24104 https://doi.org/10.1002/jcp.24104.

4. Ahuja, A.K., Jodkowska, K., Teloni, F., Bizard, A.H., Zellweger, R., Herrador, R., Ortega, S., Hickson, I.D., Altmeyer, M., Mendez, J., et al. (2016). A short G1 phase imposes constitutive replication stress and fork remodelling in mouse embryonic stem cells. Nat Commun *7*. https://doi.org/10.1038/ncomms10660.

5. Vitale, I., Manic, G., De Maria, R., Kroemer, G., and Galluzzi, L. (2017). DNA Damage in Stem Cells. Preprint at Cell Press, https://doi.org/10.1016/j.molcel.2017.04.006 https://doi.org/10.1016/j.molcel.2017.04.006.

6. Guo, Z., Kozlov, S., Lavin, M.F., Person, M.D., and Paull, T.T. (2010). ATM Activation by Oxidative Stress. Science (1979) *330*, 517–521. https://doi.org/10.1126/science.1192912.

7. Guo, Z., Deshpande, R., and Paull, T.T. (2010). ATM activation in the presence of oxidative stress . Cell Cycle *9*, 4805–4811. https://doi.org/10.4161/cc.9.24.14323.

8. Schneider, J.G., Finck, B.N., Ren, J., Standley, K.N., Takagi, M., Maclean, K.H., Bernal-Mizrachi, C., Muslin, A.J., Kastan, M.B., and Semenkovich, C.F. (2006). ATM-dependent suppression of stress signaling reduces vascular disease in metabolic syndrome. Cell Metab *4*, 377–389. https://doi.org/10.1016/j.cmet.2006.10.002.

9. Ditch, S., and Paull, T.T. (2012). The ATM protein kinase and cellular redox signaling: beyond the DNA damage response. Trends Biochem Sci *37*, 15–22. https://doi.org/10.1016/j.tibs.2011.10.002.

10. Matsuoka, S., Ballif, B.A., Smogorzewska, A., McDonald, E.R., Hurov, K.E., Luo, J., Bakalarski, C.E., Zhao, Z., Solimini, N., Lerenthal, Y., et al. (2007). ATM and ATR Substrate Analysis Reveals Extensive Protein Networks Responsive to DNA Damage. Science (1979) *316*, 1160–1166. https://doi.org/10.1126/science.1140321.

11. Zou, L., and Elledge, S.J. (2003). Sensing DNA Damage Through ATRIP Recognition of RPA-ssDNA Complexes. Science (1979) *300*, 1542–1548. https://doi.org/10.1126/science.1083430.

12. Shiotani, B., and Zou, L. (2009). Single-Stranded DNA Orchestrates an ATM-to-ATR Switch at DNA Breaks. Mol Cell *33*, 547–558. https://doi.org/10.1016/j.molcel.2009.01.024.

13. Brown, E.J., and Baltimore, D. (2000). ATR disruption leads to chromosomal fragmentation and early embryonic lethality. Genes Dev *14*, 397–402.

14. Ruzankina, Y., Pinzon-Guzman, C., Asare, A., Ong, T., Pontano, L., Cotsarelis, G., Zediak, V.P., Velez, M., Bhandoola, A., and Brown, E.J. (2007). Deletion of the Developmentally Essential Gene ATR in Adult Mice Leads to Age-Related Phenotypes and Stem Cell Loss. Cell Stem Cell *1*, 113–126. https://doi.org/10.1016/j.stem.2007.03.002.

15. Morrison, S.J., and Spradling, A.C. Stem cells and niches: mechanisms that promote stem cell maintenance throughout life.

16. Pennings, S., Liu, K.J., and Qian, H. (2018). The stem cell niche: Interactions between stem cells and their environment. Preprint at Hindawi Limited, https://doi.org/10.1155/2018/4879379 https://doi.org/10.1155/2018/4879379.

17. Xie, T., and Li, L. (2007). Stem cells and their niche: An inseparable relationship. In Development, pp. 2001–2006. https://doi.org/10.1242/dev.002022.

18. Reinwald, Y., Bratt, J., and El Haj, A. (2016). Pluripotent Stem Cells and Their Dynamic Niche. In Pluripotent Stem Cells - From the Bench to the Clinic (InTech). https://doi.org/10.5772/62671.

19. Engler, A.J., Sen, S., Sweeney, H.L., and Discher, D.E. (2006). Matrix Elasticity Directs Stem Cell Lineage Specification. Cell *126*, 677–689. https://doi.org/10.1016/j.cell.2006.06.044.

20. Sthanam, L.K., Saxena, N., Mistari, V.K., Roy, T., Jadhav, S.R., and Sen, S. (2019). Initial Priming on Soft Substrates Enhances Subsequent Topography-Induced Neuronal Differentiation in ESCs but Not in MSCs. ACS Biomater Sci Eng *5*, 180–192. https://doi.org/10.1021/acsbiomaterials.8b00313.

21. Dos Santos, Á., and Toseland, C.P. (2021). Regulation of nuclear mechanics and the impact on dna damage. Int J Mol Sci *22*, 1–18. https://doi.org/10.3390/ijms22063178.

22. Shah, P., Wolf, K., and Lammerding, J. (2017). Bursting the Bubble – Nuclear Envelope Rupture as a Path to Genomic Instability? Preprint at Elsevier Ltd, https://doi.org/10.1016/j.tcb.2017.02.008 https://doi.org/10.1016/j.tcb.2017.02.008.

23. Chalut, K.J., Höpfler, M., Lautenschläger, F., Boyde, L., Chan, C.J., Ekpenyong, A., Martinez-Arias, A., and Guck, J. (2012). Chromatin Decondensation and Nuclear Softening Accompany Nanog Downregulation in Embryonic Stem Cells. Biophys J *103*, 2060–2070. https://doi.org/10.1016/j.bpj.2012.10.015.

24. Pagliara, S., Franze, K., McClain, C.R., Wylde, G.W., Fisher, C.L., Franklin, R.J.M., Kabla, A.J., Keyser, U.F., and Chalut, K.J. (2014). Auxetic nuclei in embryonic stem cells exiting pluripotency. Nat Mater *13*, 638–644. https://doi.org/10.1038/nmat3943.

25. Gonzalo, S. (2014). DNA damage and lamins. Adv Exp Med Biol *773*, 377–399. https://doi.org/10.1007/978-1-4899-8032-8_17.

26. Gonzalez-Suarez, I., Redwood, A.B., Perkins, S.M., Vermolen, B., Lichtensztejin, D., Grotsky, D.A., Morgado-Palacin, L., Gapud, E.J., Sleckman, B.P., Sullivan, T., et al. (2009). Novel roles for A-type lamins in telomere biology and the DNA damage response pathway. EMBO Journal *28*, 2414–2427. https://doi.org/10.1038/emboj.2009.196.

27. Graziano, S., Coll-Bonfill, N., Teodoro-Castro, B., Kuppa, S., Jackson, J., Shashkova, E., Mahajan, U., Vindigni, A., Antony, E., and Gonzalo, S. (2021). Lamin A/C recruits ssDNA

protective proteins RPA and RAD51 to stalled replication forks to maintain fork stability. Journal of Biological Chemistry *297*, 101301. https://doi.org/10.1016/j.jbc.2021.101301.

28. Gibbs-Seymour, I., Markiewicz, E., Bekker-Jensen, S., Mailand, N., and Hutchison, C.J. (2015). Lamin A/C-dependent interaction with 53BP1 promotes cellular responses to DNA damage. Aging Cell *14*, 162–169. https://doi.org/10.1111/acel.12258.

29. Zhang, B., Yang, Y., Keyimu, R., Hao, J., Zhao, Z., and Ye, R. (2019). The role of lamin A/C in mesenchymal stem cell differentiation. Preprint at Springer Netherlands, https://doi.org/10.1007/s13105-019-00661-z https://doi.org/10.1007/s13105-019-00661-z.

30. Lammerding, J., Schulze, P.C., Takahashi, T., Kozlov, S., Sullivan, T., Kamm, R.D., Stewart, C.L., and Lee, R.T. (2004). Lamin A/C deficiency causes defective nuclear mechanics and mechanotransduction. Journal of Clinical Investigation *113*, 370–378. https://doi.org/10.1172/JCI200419670.

31. Sehgal, P., Chaturvedi, P., Kumaran, R.I., Kumar, S., and Parnaik, V.K. (2013). Lamin A/C Haploinsufficiency Modulates the Differentiation Potential of Mouse Embryonic Stem Cells. PLoS One *8*, e57891. https://doi.org/10.1371/journal.pone.0057891.

32. Swift, J., Ivanovska, I.L., Buxboim, A., Harada, T., Dingal, P.C.D.P., Pinter, J., Pajerowski, J.D., Spinler, K.R., Shin, J.W., Tewari, M., et al. (2013). Nuclear lamin-A scales with tissue stiffness and enhances matrix-directed differentiation. Science (1979) *341*. https://doi.org/10.1126/science.1240104.

33. Wang, Y., Elsherbiny, A., Kessler, L., Cordero, J., Shi, H., Serke, H., Lityagina, O., Trogisch, F.A., Mohammadi, M.M., El-Battrawy, I., et al. (2022). Lamin A/C-dependent chromatin architecture safeguards naïve pluripotency to prevent aberrant cardiovascular cell fate and function. Nat Commun *13*. https://doi.org/10.1038/s41467-022-34366-7.

34. Nigg, E.A. (1992). Assembly and cell cycle dynamics of the nuclear lamina. Semin Cell Biol *3*, 245–253. https://doi.org/10.1016/1043-4682(92)90026-R.

35. Nakamura, M., Yamada, M., Ohsawa, T., Morisawa, H., Nishine, T., Nishimura, O., and Toda, T. (2006). Phosphoproteomic profiling of human SH-SY5Y neuroblastoma cells during response to 6-hydroxydopamine-induced oxidative stress. Biochimica et Biophysica Acta (BBA) - Molecular Cell Research *1763*, 977–989. https://doi.org/10.1016/j.bbamcr.2006.07.008.

36. Shimi, T., and Goldman, R.D. (2014). Nuclear Lamins and Oxidative Stress in Cell Proliferation and Longevity. In, pp. 415–430. https://doi.org/10.1007/978-1-4899-8032-8_19.

37. Virtanen, L., Holm, E., Halme, M., West, G., Lindholm, F., Gullmets, J., Irjala, J., Heliö, T., Padzik, A., Meinander, A., et al. (2023). Lamin A/C phosphorylation at serine 22 is a conserved heat shock response to regulate nuclear adaptation during stress. J Cell Sci *136*. https://doi.org/10.1242/jcs.259788.

38. Buxboim, A., Swift, J., Irianto, J., Spinler, K.R., Dingal, P.C.D.P., Athirasala, A., Kao, Y.R.C., Cho, S., Harada, T., Shin, J.W., et al. (2014). Matrix elasticity regulates lamin-A,C phosphorylation and turnover with feedback to actomyosin. Current Biology *24*, 1909–1917. https://doi.org/10.1016/j.cub.2014.07.001.

39. Das, A., Barai, A., Monteiro, M., Kumar, S., and Sen, S. (2019). Nuclear softening is essential for protease-independent migration. Matrix Biology *82*, 4–19. https://doi.org/10.1016/j.matbio.2019.01.001.

40. Lammerding, J., and Wolf, K. (2016). Nuclear envelope rupture: Actin fibers are putting the squeeze on the nucleus. Journal of Cell Biology *215*. https://doi.org/10.1083/jcb.201609102.

41. Lim, S., Quinton, R.J., and Ganem, N.J. (2016). Nuclear envelope rupture drives genome instability in cancer. Preprint at American Society for Cell Biology, https://doi.org/10.1091/mbc.E16-02-0098 https://doi.org/10.1091/mbc.E16-02-0098.

42. Denais, C.M., Gilbert, R.M., Isermann, P., McGregor, A.L., te Lindert, M., Weigelin, B., Davidson, P.M., Friedl, P., Wolf, K., and Lammerding, J. (2016). Nuclear envelope rupture and repair during cancer cell migration. Science (1979) *352*, 353–358. https://doi.org/10.1126/science.aad7297.

43. Kidiyoor, G.R., Li, Q., Bastianello, G., Bruhn, C., Giovannetti, I., Mohamood, A., Beznoussenko, G. V., Mironov, A., Raab, M., Piel, M., et al. (2020). ATR is essential for preservation of cell mechanics and nuclear integrity during interstitial migration. Nat Commun *11*. https://doi.org/10.1038/s41467-020-18580-9.

44. Kumar, A., Mazzanti, M., Mistrik, M., Kosar, M., Beznoussenko, G. V., Mironov, A.A., Garrè, M., Parazzoli, D., Shivashankar, G. V., Scita, G., et al. (2014). ATR mediates a checkpoint at the nuclear envelope in response to mechanical stress. Cell *158*, 633–646. https://doi.org/10.1016/j.cell.2014.05.046.

45. Li, F., Lo, T.Y., Miles, L., Wang, Q., Noristani, H.N., Li, D., Niu, J., Trombley, S., Goldshteyn, J.I., Wang, C., et al. (2021). The Atr-Chek1 pathway inhibits axon regeneration in response to Piezo-dependent mechanosensation. Nat Commun *12*, 3845. https://doi.org/10.1038/s41467-021-24131-7.

46. Bastianello, G., Porcella, G., Beznoussenko, G. V, Kidiyoor, G., Ascione, F., Li, Q., Cattaneo, A., Matafora, V., Disanza, A., Quarto, M., et al. (2023). Cell stretching activates an ATM mechano-transduction pathway that remodels cytoskeleton and chromatin. Cell Rep *42*, 113555. https://doi.org/10.1016/j.celrep.2023.113555.

47. Shah, P., McGuigan, C.W., Cheng, S., Vanpouille-Box, C., Demaria, S., Weiss, R.S., and Lammerding, J. (2022). ATM Modulates Nuclear Mechanics by Regulating Lamin A Levels. Front Cell Dev Biol *10*. https://doi.org/10.3389/fcell.2022.875132.

48. Sthanam, L.K., Barai, A., Rastogi, A., Mistari, V.K., Maria, A., Kauthale, R., Gatne, M., and Sen, S. (2017). Biophysical regulation of mouse embryonic stem cell fate and genomic integrity by feeder derived matrices. Biomaterials *119*, 9–22. https://doi.org/10.1016/j.biomaterials.2016.12.006.

49. Ahuja, A.K., Jodkowska, K., Teloni, F., Bizard, A.H., Zellweger, R., Herrador, R., Ortega, S., Hickson, I.D., Altmeyer, M., Mendez, J., et al. (2016). A short G1 phase imposes constitutive replication stress and fork remodelling in mouse embryonic stem cells. Nat Commun *7*. https://doi.org/10.1038/ncomms10660.

50. Tse, J.R., and Engler, A.J. (2010). Preparation of hydrogel substrates with tunable mechanical properties. Preprint, https://doi.org/10.1002/0471143030.cb1016s47 https://doi.org/10.1002/0471143030.cb1016s47.

51. Das, A., Monteiro, M., Barai, A., Kumar, S., and Sen, S. (2017). MMP proteolytic activity regulates cancer invasiveness by modulating integrins. Sci Rep *7*. https://doi.org/10.1038/s41598-017-14340-w.

52. Mackay, J.L., and Kumar, S. (2013). Cell Imaging Techniques. *931*, 313–329. https://doi.org/10.1007/978-1-62703-056-4.

53. Chuykin, I.A., Lianguzova, M.S., Pospelova, T. V, and Pospelov, V.A. (2008). Activation of DNA damage response signaling in mouse embryonic stem cells. Cell Cycle *7*, 2922–2928. https://doi.org/10.4161/cc.7.18.6699.

54. Ward, I.M., Minn, K., and Chen, J. (2004). UV-induced Ataxia-telangiectasia-mutated and Rad3-related (ATR) Activation Requires Replication Stress. Journal of Biological Chemistry *279*, 9677–9680. https://doi.org/10.1074/jbc.C300554200.

55. Banáth, J.P., Bañuelos, C.A., Klokov, D., MacPhail, S.M., Lansdorp, P.M., and Olive, P.L. (2009). Explanation for excessive DNA single-strand breaks and endogenous repair foci in pluripotent mouse embryonic stem cells. Exp Cell Res *315*, 1505–1520. https://doi.org/10.1016/j.yexcr.2008.12.007.

56. Dormond, O., Ponsonnet, L., Hasmim, M., Foletti, A., and Rüegg, C. (2004). Manganese-induced integrin affinity maturation promotes recruitment of αVβ3 integrin to focal adhesions in endothelial cells: evidence for a role of phosphatidylinositol 3-kinase and Src. Thromb Haemost *92*, 151–161. https://doi.org/10.1160/TH03-11-0728.

57. Cluzel, C., Saltel, F., Lussi, J., Paulhe, F., Imhof, B.A., and Wehrle-Haller, B. (2005). The mechanisms and dynamics of αvβ3 integrin clustering in living cells. J Cell Biol *171*, 383–392. https://doi.org/10.1083/jcb.200503017.

58. Lu, F., Zhu, L., Bromberger, T., Yang, J., Yang, Q., Liu, J., Plow, E.F., Moser, M., and Qin, J. (2022). Mechanism of integrin activation by talin and its cooperation with kindlin. Nat Commun *13*, 2362. https://doi.org/10.1038/s41467-022-30117-w.

59. Evans, N., Minelli, C., Gentleman, E., LaPointe, V., Patankar, S., Kallivretaki, M., Chen, X., Roberts, C., and Stevens, M. (2009). Substrate stiffness affects early differentiation events in embryonic stem cells. Eur Cell Mater *18*, 1–14. https://doi.org/10.22203/eCM.v018a01.

60. Chowdhury, F., Li, Y., Poh, Y.C., Yokohama-Tamaki, T., Wang, N., and Tanaka, T.S. (2010). Soft substrates promote homogeneous self-renewal of embryonic stem cells via downregulating cell-matrix tractions. PLoS One *5*. https://doi.org/10.1371/journal.pone.0015655.

61. Sthanam, L.K., Roy, T., Patwardhan, S., Shukla, A., Sharma, S., Shinde, P. V., Kale, H.T., Chandra Shekar, P., Kondabagil, K., and Sen, S. (2022). MMP modulated differentiation of mouse embryonic stem cells on engineered cell derived matrices. Biomaterials *280*. https://doi.org/10.1016/j.biomaterials.2021.121268.

62. Nichols, J., Zevnik, B., Anastassiadis, K., Niwa, H., Klewe-Nebenius, D., Chambers, I., Schöler, H., and Smith, A. (1998). Formation of Pluripotent Stem Cells in the Mammalian Embryo Depends on the POU Transcription Factor Oct4. Cell *95*, 379–391. https://doi.org/10.1016/S0092-8674(00)81769-9.

63. Niwa, H., Miyazaki, J., and Smith, A.G. (2000). Quantitative expression of Oct-3/4 defines differentiation, dedifferentiation or self-renewal of ES cells. Nat Genet *24*, 372–376. https://doi.org/10.1038/74199.

64. Avilion, A.A., Nicolis, S.K., Pevny, L.H., Perez, L., Vivian, N., and Lovell-Badge, R. (2003). Multipotent cell lineages in early mouse development depend on SOX2 function. Genes Dev *17*, 126–140. https://doi.org/10.1101/gad.224503.

65. Mitsui, K., Tokuzawa, Y., Itoh, H., Segawa, K., Murakami, M., Takahashi, K., Maruyama, M., Maeda, M., and Yamanaka, S. (2003). The Homeoprotein Nanog Is Required for Maintenance of Pluripotency in Mouse Epiblast and ES Cells. Cell *113*, 631–642. https://doi.org/10.1016/S0092-8674(03)00393-3.

66. Chambers, I., Colby, D., Robertson, M., Nichols, J., Lee, S., Tweedie, S., and Smith, A. (2003). Functional Expression Cloning of Nanog, a Pluripotency Sustaining Factor in Embryonic Stem Cells. Cell *113*, 643–655. https://doi.org/10.1016/S0092-8674(03)00392-1.

67. Li, Y., McClintick, J., Zhong, L., Edenberg, H.J., Yoder, M.C., and Chan, R.J. (2005). Murine embryonic stem cell differentiation is promoted by SOCS-3 and inhibited by the zinc finger transcription factor Klf4. Blood *105*, 635–637. https://doi.org/10.1182/blood-2004-07-2681.

68. Anderson, W.J., Zhou, Q., Alcalde, V., Kaneko, O.F., Blank, L.J., Sherwood, R.I., Guseh, J.S., Rajagopal, J., and Melton, D.A. (2008). Genetic targeting of the endoderm with claudin-6CreER. Developmental Dynamics *237*, 504–512. https://doi.org/10.1002/dvdy.21437.

69. Enikanolaiye, A., Larivière, N., Troy, T.-C., Arabzadeh, A., Atasoy, E., and Turksen, K. (2010). Involucrin–claudin-6 tail deletion mutant (CΔ206) transgenic mice: a model of delayed epidermal permeability barrier formation and repair. Dis Model Mech *3*, 167–180. https://doi.org/10.1242/dmm.002634.

70. Soudais, C., Bielinska, M., Heikinheimo, M., MacArthur, C.A., Narita, N., Saffitz, J.E., Simon, M.C., Leiden, J.M., and Wilson, D.B. (1995). Targeted mutagenesis of the transcription factor GATA-4 gene in mouse embryonic stem cells disrupts visceral endoderm differentiation in vitro. Development *121*, 3877–3888. https://doi.org/10.1242/dev.121.11.3877.

71. Spence, J.R., Lange, A.W., Lin, S.-C.J., Kaestner, K.H., Lowy, A.M., Kim, I., Whitsett, J.A., and Wells, J.M. (2009). Sox17 Regulates Organ Lineage Segregation of Ventral Foregut Progenitor Cells. Dev Cell *17*, 62–74. https://doi.org/10.1016/j.devcel.2009.05.012.

72. Levinson-Dushnik, M., and Benvenisty, N. (1997). Involvement of Hepatocyte Nuclear Factor 3 in Endoderm Differentiation of Embryonic Stem Cells. Mol Cell Biol *17*, 3817–3822. https://doi.org/10.1128/MCB.17.7.3817.

73. Lee, C.S., Friedman, J.R., Fulmer, J.T., and Kaestner, K.H. (2005). The initiation of liver development is dependent on Foxa transcription factors. Nature *435*, 944–947. https://doi.org/10.1038/nature03649.

74. Chapman, D.L., and Papaioannou, V.E. (1998). Three neural tubes in mouse embryos with mutations in the T-box gene Tbx6. Nature *391*, 695–697. https://doi.org/10.1038/35624.

75. Takemoto, T., Uchikawa, M., Yoshida, M., Bell, D.M., Lovell-Badge, R., Papaioannou, V.E., and Kondoh, H. (2011). Tbx6-dependent Sox2 regulation determines neural or mesodermal fate in axial stem cells. Nature *470*, 394–398. https://doi.org/10.1038/nature09729.

76. Thisse, B., Messal, M. El, and Perrin-Schmitt, F. (1987). The twist gene: isolation of a Drosophila zygotic gene necessary for the establishment of dorsoventral pattern. Nucleic Acids Res *15*, 3439–3453. https://doi.org/10.1093/nar/15.8.3439.

77. Ota, M.S., Loebel, D.A.F., O'Rourke, M.P., Wong, N., Tsoi, B., and Tam, P.P.L. (2004). Twist is required for patterning the cranial nerves and maintaining the viability of mesodermal cells. Developmental Dynamics *230*, 216–228. https://doi.org/10.1002/dvdy.20047.

78. Soo, K., O'Rourke, M.P., Khoo, P.-L., Steiner, K.A., Wong, N., Behringer, R.R., and Tam, P.P.L. (2002). Twist Function Is Required for the Morphogenesis of the Cephalic Neural Tube and the Differentiation of the Cranial Neural Crest Cells in the Mouse Embryo. Dev Biol *247*, 251–270. https://doi.org/10.1006/dbio.2002.0699.

79. Murray, S.A., and Gridley, T. (2006). Snail family genes are required for left–right asymmetry determination, but not neural crest formation, in mice. Proceedings of the National Academy of Sciences *103*, 10300–10304. https://doi.org/10.1073/pnas.0602234103.

80. Ashraf, S.I., Hu, X., Roote, J., and Ip, Y.T. (1999). The mesoderm determinant Snail collaborates with related zinc-finger proteins to control Drosophila neurogenesis. EMBO J *18*, 6426–6438. https://doi.org/10.1093/emboj/18.22.6426.

81. Lobo, M.V.T., Arenas, M.I., Alonso, F.J.M., Gomez, G., Bazán, E., Paíno, C.L., Fernández, E., Fraile, B., Paniagua, R., Moyano, A., et al. (2004). Nestin, a neuroectodermal stem cell marker molecule, is expressed in Leydig cells of the human testis and in some specific cell types from human testicular tumours. Cell Tissue Res *316*, 369–376. https://doi.org/10.1007/s00441-003-0848-4.

82. Zou, L., Kidwai, F.K., Kopher, R.A., Motl, J., Kellum, C.A., Westendorf, J.J., and Kaufman, D.S. (2015). Use of RUNX2 Expression to Identify Osteogenic Progenitor Cells Derived from Human Embryonic Stem Cells. Stem Cell Reports *4*, 190–198. https://doi.org/10.1016/j.stemcr.2015.01.008.

83. Nahaboo, W., Eski, S.E., Despin-Guitard, E., Vermeersch, M., Versaevel, M., Saykali, B., Monteyne, D., Gabriele, S., Magin, T.M., Schwarz, N., et al. (2022). Keratin filaments mediate the expansion of extra-embryonic membranes in the post-gastrulation mouse embryo. EMBO J *41*. https://doi.org/10.15252/embj.2021108747.

84. Kemp, C., Willems, E., Abdo, S., Lambiv, L., and Leyns, L. (2005). Expression of all Wnt genes and their secreted antagonists during mouse blastocyst and postimplantation development. Developmental Dynamics *233*, 1064–1075. https://doi.org/10.1002/dvdy.20408.

85. Ralston, A., Cox, B.J., Nishioka, N., Sasaki, H., Chea, E., Rugg-Gunn, P., Guo, G., Robson, P., Draper, J.S., and Rossant, J. (2010). Gata3 regulates trophoblast development downstream of Tead4 and in parallel to Cdx2. Development *137*, 395–403. https://doi.org/10.1242/dev.038828.

86. Raab, M., Gentili, M., de Belly, H., Thiam, H.-R., Vargas, P., Jimenez, A.J., Lautenschlaeger, F., Voituriez, R., Lennon-Duménil, A.-M., Manel, N., et al. (2016). ESCRT III repairs nuclear envelope ruptures during cell migration to limit DNA damage and cell death. Science (1979) *352*, 359–362. https://doi.org/10.1126/science.aad7611.

87. Cho, S., Vashisth, M., Abbas, A., Majkut, S., Vogel, K., Xia, Y., Ivanovska, I.L., Irianto, J., Tewari, M., Zhu, K., et al. (2019). Mechanosensing by the Lamina Protects against Nuclear Rupture,

DNA Damage, and Cell-Cycle Arrest. Dev Cell *49*, 920-935.e5. https://doi.org/10.1016/j.devcel.2019.04.020.

88. Muncie, J.M., Ayad, N.M.E., Lakins, J.N., Xue, X., Fu, J., and Weaver, V.M. (2020). Mechanical Tension Promotes Formation of Gastrulation-like Nodes and Patterns Mesoderm Specification in Human Embryonic Stem Cells. Dev Cell *55*, 679-694.e11. https://doi.org/10.1016/j.devcel.2020.10.015.

89. Mamidi, A., Prawiro, C., Seymour, P.A., de Lichtenberg, K.H., Jackson, A., Serup, P., and Semb, H. (2018). Mechanosignalling via integrins directs fate decisions of pancreatic progenitors. Nature *564*, 114–118. https://doi.org/10.1038/s41586-018-0762-2.

90. Nagaria, P., Robert, C., and Rassool, F. V. (2013). DNA double-strand break response in stem cells: Mechanisms to maintain genomic integrity. Preprint, https://doi.org/10.1016/j.bbagen.2012.09.001 https://doi.org/10.1016/j.bbagen.2012.09.001.

91. Lin, T., Chao, C., Saito, S., Mazur, S.J., Murphy, M.E., Appella, E., and Xu, Y. (2005). p53 induces differentiation of mouse embryonic stem cells by suppressing Nanog expression. Nat Cell Biol *7*, 165–171. https://doi.org/10.1038/ncb1211.

92. Qin, H., Yu, T., Qing, T., Liu, Y., Zhao, Y., Cai, J., Li, J., Song, Z., Qu, X., Zhou, P., et al. (2007). Regulation of Apoptosis and Differentiation by p53 in Human Embryonic Stem Cells. Journal of Biological Chemistry *282*, 5842–5852. https://doi.org/10.1074/jbc.M610464200.

93. Tichy*Elisia D. And PeterJ.Stambrook (2009). DNA Repair in Murine Embryonic Stem Cells and Differentiated Cells. Cell *314*, 1929–1936. https://doi.org/10.1016/j.yexcr.2008.02.007.DNA.

94. Staudt, D., and Stainier, D. (2012). Uncovering the Molecular and Cellular Mechanisms of Heart Development Using the Zebrafish. Annu Rev Genet *46*, 397–418. https://doi.org/10.1146/annurev-genet-110711-155646.

95. Kovacs, M.T., Vallette, M., Wiertsema, P., Dingli, F., Loew, D., de Freitas Nader, G.P., Piel, M., and Ceccaldi, R. (2023). DNA damage induces nuclear envelope rupture through ATR-mediated phosphorylation of lamin A/C. Mol Cell *83*, 3659-3668.e10. https://doi.org/10.1016/j.molcel.2023.09.023.

96. Bonello-Palot, N., Simoncini, S., Robert, S., Bourgeois, P., Sabatier, F., Levy, N., Dignat-George, F., and Badens, C. (2014). Prelamin A accumulation in endothelial cells induces premature senescence and functional impairment. Atherosclerosis *237*, 45–52. https://doi.org/10.1016/j.atherosclerosis.2014.08.036.

97. Liu, B., Wang, J., Chan, K.M., Tjia, W.M., Deng, W., Guan, X., Huang, J., Li, K.M., Chau, P.Y., Chen, D.J., et al. (2005). Genomic instability in laminopathy-based premature aging. Nat Med *11*, 780–785. https://doi.org/10.1038/nm1266.

98. Graziano, S., Kreienkamp, R., Coll-Bonfill, , Nuria, and Gonzalo, S. (2018). Causes and consequences of genomic instability in laminopathies: Replication stress and interferon response. Nucleus *9*, 289–306. https://doi.org/10.1080/19491034.2018.1454168.

99. dos Santos, Á., Cook, A.W., Gough, R.E., Schilling, M., Olszok, N.A., Brown, I., Wang, L., Aaron, J., Martin-Fernandez, M.L., Rehfeldt, F., et al. (2021). DNA damage alters nuclear mechanics

through chromatin reorganization. Nucleic Acids Res *49*, 340–353. https://doi.org/10.1093/nar/gkaa1202.

100. Moiseeva, T.N., Yin, Y., Calderon, M.J., Qian, C., Schamus-Haynes, S., Sugitani, N., Osmanbeyoglu, H.U., Rothenberg, E., Watkins, S.C., and Bakkenist, C.J. (2019). An ATR and CHK1 kinase signaling mechanism that limits origin firing during unperturbed DNA replication. Proceedings of the National Academy of Sciences *116*, 13374–13383. https://doi.org/10.1073/pnas.1903418116.

101. Zhao, H., and Piwnica-Worms, H. (2001). ATR-Mediated Checkpoint Pathways Regulate Phosphorylation and Activation of Human Chk1. Mol Cell Biol *21*, 4129–4139. https://doi.org/10.1128/MCB.21.13.4129-4139.2001.

102. Caldecott, K.W. (2022). DNA single-strand break repair and human genetic disease. Trends Cell Biol *32*, 733–745. https://doi.org/10.1016/j.tcb.2022.04.010.

103. Tubbs, A., and Nussenzweig, A. (2017). Endogenous DNA Damage as a Source of Genomic Instability in Cancer. Cell *168*, 644–656. https://doi.org/10.1016/j.cell.2017.01.002.

104. Ciccia, A., and Elledge, S.J. (2010). The DNA Damage Response: Making It Safe to Play with Knives. Mol Cell *40*, 179–204. https://doi.org/10.1016/j.molcel.2010.09.019.

105. Hayashi, Y., Furue, M.K., Okamoto, T., Ohnuma, K., Myoishi, Y., Fukuhara, Y., Abe, T., Sato, J.D., Hata, R.-I., and Asashima, M. (2007). Integrins Regulate Mouse Embryonic Stem Cell Self-Renewal. Stem Cells *25*, 3005–3015. https://doi.org/10.1634/stemcells.2007-0103.

106. Suh, H.N., and Han, H.J. (2011). Collagen I regulates the self-renewal of mouse embryonic stem cells through α2β1 integrin- and DDR1-dependent Bmi-1. J Cell Physiol *226*, 3422–3432. https://doi.org/10.1002/jcp.22697.

107. Kang, Y., Georgiou, A.I., MacFarlane, R.J., Klontzas, M.E., Heliotis, M., Tsiridis, E., and Mantalaris, A. (2017). Fibronectin stimulates the osteogenic differentiation of murine embryonic stem cells. J Tissue Eng Regen Med *11*, 1929–1940. https://doi.org/10.1002/term.2090.

108. Brafman, D.A., Phung, C., Kumar, N., and Willert, K. (2013). Regulation of endodermal differentiation of human embryonic stem cells through integrin-ECM interactions. Cell Death Differ *20*, 369–381. https://doi.org/10.1038/cdd.2012.138.

109. Pimton, P., Sarkar, S., Sheth, N., Perets, A., Marcinkiewicz, C., Lazarovici, P., and Lelkes, P.I. (2011). Fibronectin-mediated upregulation of α5β1 integrin and cell adhesion during differentiation of mouse embryonic stem cells. Cell Adh Migr *5*, 73–82. https://doi.org/10.4161/cam.5.1.13704.

110. Zhu, Y., Li, X., Janairo, R.R.R., Kwong, G., Tsou, A.D., Chu, J.S., Wang, A., Yu, J., Wang, D., and Li, S. (2019). Matrix stiffness modulates the differentiation of neural crest stem cells in vivo. J Cell Physiol *234*, 7569–7578. https://doi.org/10.1002/jcp.27518.

111. Xia, Y., Ivanovska, I.L., Zhu, K., Smith, L., Irianto, J., Pfeifer, C.R., Alvey, C.M., Ji, J., Liu, D., Cho, S., et al. (2018). Nuclear rupture at sites of high curvature compromises retention of DNA repair factors. Journal of Cell Biology *217*, 3796–3808. https://doi.org/10.1083/jcb.201711161.

112. Shah, P., Hobson, C.M., Cheng, S., Colville, M.J., Paszek, M.J., Superfine, R., and Lammerding, J. (2021). Nuclear Deformation Causes DNA Damage by Increasing Replication Stress. Current Biology *31*, 753-765.e6. https://doi.org/10.1016/j.cub.2020.11.037.

113. Puri, P.L., Bhakta, K., Wood, L.D., Costanzo, A., Zhu, J., and Wang, J.Y.J. (2002). A myogenic differentiation checkpoint activated by genotoxic stress. Nat Genet *32*, 585–593. https://doi.org/10.1038/ng1023.

114. Larsen, B.D., Rampalli, S., Burns, L.E., Brunette, S., Dilworth, F.J., and Megeney, L.A. (2010). Caspase 3/caspase-activated DNase promote cell differentiation by inducing DNA strand breaks. Proceedings of the National Academy of Sciences *107*, 4230–4235. https://doi.org/10.1073/pnas.0913089107.

115. Smith, L.R., Irianto, J., Xia, Y., Pfeifer, C.R., and Discher, D.E. (2019). Constricted migration modulates stem cell differentiation. Mol Biol Cell *30*, 1985–1999. https://doi.org/10.1091/mbc.E19-02-0090.

116. Raz, R., Lee, C.-K., Cannizzaro, L.A., d'Eustachio, P., and Levy, D.E. (1999). Essential role of STAT3 for embryonic stem cell pluripotency. Proceedings of the National Academy of Sciences *96*, 2846–2851. https://doi.org/10.1073/pnas.96.6.2846.

117. Duval, D., Malaisé, M., Reinhardt, B., Kedinger, C., and Boeuf, H. (2004). A p38 inhibitor allows to dissociate differentiation and apoptotic processes triggered upon LIF withdrawal in mouse embryonic stem cells. Cell Death Differ *11*, 331–341. https://doi.org/10.1038/sj.cdd.4401337.

118. Duval, D., Trouillas, M., Thibault, C., Dembelé, D., Diemunsch, F., Reinhardt, B., Mertz, A.L., Dierich, A., and Bœuf, H. (2006). Apoptosis and differentiation commitment: Novel insights revealed by gene profiling studies in mouse embryonic stem cells. Cell Death Differ *13*, 564–575. https://doi.org/10.1038/sj.cdd.4401789.

119. Constantinescu, D., Gray, H.L., Sammak, P.J., Schatten, G.P., and Csoka, A.B. (2006). Lamin A/C expression is a marker of mouse and human embryonic stem cell differentiation. Stem Cells *24*, 474. https://doi.org/10.1634/stemcells.2006-erratum.2.

120. Eckersley-Maslin, M.A., Bergmann, J.H., Lazar, Z., and Spector, D.L. (2013). Lamin A/C is expressed in pluripotent mouse embryonic stem cells. Nucleus (United States) *4*, 53–60. https://doi.org/10.4161/nucl.23384.

121. Redwood, A.B., Perkins, S.M., Vanderwaal, R.P., Feng, Z., Biehl, K.J., Gonzalez-Suarez, I., Morgado-Palacin, L., Shi, W., Sage, J., Roti-Roti, J.L., et al. (2011). A dual role for A-type lamins in DNA double-strand break repair. Cell Cycle *10*, 2549–2560. https://doi.org/10.4161/cc.10.15.16531.

122. Mahen, R., Hattori, H., Lee, M., Sharma, P., Jeyasekharan, A.D., and Venkitaraman, A.R. (2013). A-Type Lamins Maintain the Positional Stability of DNA Damage Repair Foci in Mammalian Nuclei. PLoS One *8*, e61893. https://doi.org/10.1371/journal.pone.0061893.

123. Aladjem, M.I., Spike, B.T., Rodewald, L.W., Hope, T.J., Klemm, M., Jaenisch, R., and Wahl, G.M. (1998). ES cells do not activate p53-dependent stress responses and undergo p53-independent apoptosis in response to DNA damage. Current Biology *8*, 145–155. https://doi.org/10.1016/S0960-9822(98)70061-2.

124. Tichy, E.D. (2011). Mechanisms maintaining genomic integrity in embryonic stem cells and induced pluripotent stem cells. Preprint, https://doi.org/10.1258/ebm.2011.011107 https://doi.org/10.1258/ebm.2011.011107.

125. Atashpaz, S., Samadi Shams, S., Gonzalez, J.M., Sebestyén, E., Arghavanifard, N., Gnocchi, A., Albers, E., Minardi, S., Faga, G., Soffientini, P., et al. (2020). ATR expands embryonic stem cell fate potential in response to replication stress. Elife *9*. https://doi.org/10.7554/eLife.54756.

Figures and Figure Legends

Figure 1

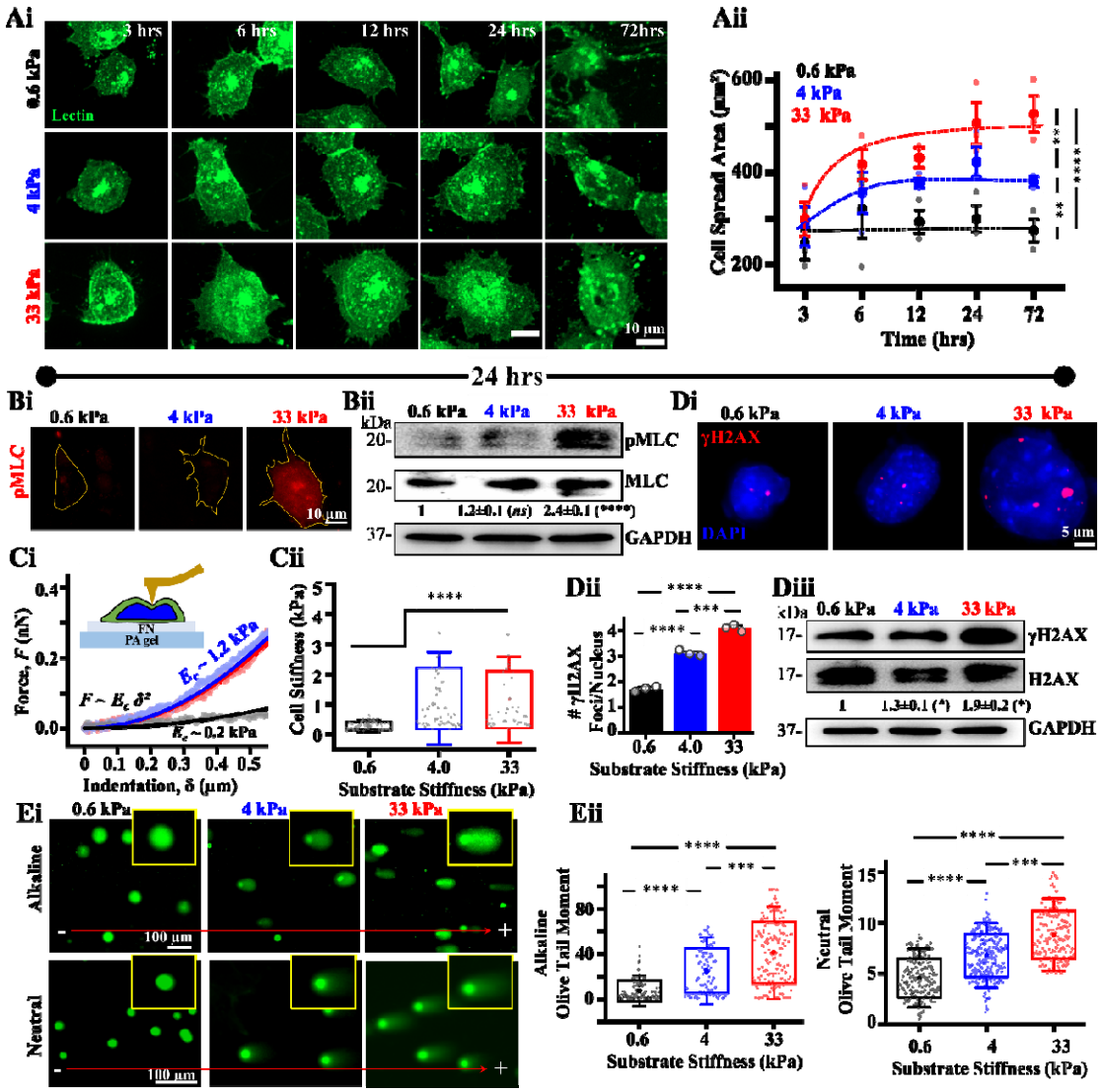

Figure 1: Association of mechanoadaptation and DNA damage in mouse embryonic stem cells (mESCs): (Ai, ii) Representative lectin-stained images of mESCs on fibronectin (FN)-coated polyacrylamide (PA) gels of varying stiffness post 3, 6, 12, 24 hours and 72 hours of seeding and quantification of cell spreading (cells per condition across N = 3 independent experiments). Scale Bar = 10μm. Error bars represent SD. Two- way ANOVA with Tukey's test was used for comparing means (** -value 0.01, **** -value 0.0001). **(Bi, ii)** Assessment of pMLC expression in mESCs cultured on PA gels for 24 hours based on immunofluorescence and western blotting showing mean ±SEM of pMLC/MLC (N = 3 independent experiments). Two- way ANOVA with Tukey's test was used for comparing means with respect to 0.6 kPa conditions (**** -value 0.0001). Scale Bar = 10μm. **(Ci-iii)** Measurement of mESC cortical stiffness using atomic force microscopy (AFM) after 24 hrs in culture. Cells were probed with a soft pyramidal probe and first 500 nm of the raw force-indentation curves were fitted with Hertz model to estimate cortical stiffness (cells per condition across N = 3 independent experiments). One- way ANOVA with Tukey's

test was used for comparing means (**** p-value ≤0.0001). **(Di-iii)** Quantification of DNA damage in mESCs cultured on PA gels for 24 hrs. DNA damage was assessed by co-staining cells with DAPI and γH2AX and counting γH2AX foci per nucleus ($n \geq 50$ nuclei per condition across N = 3 independent experiments) and western blotting of whole cell lysates showing mean ±SEM of γH2AX/H2AX (N = 3 independent experiments). Two- way ANOVA with Tukey's test was used for comparing means with respect to 0.6 kPa conditions (*p-value ≤0.05). Error bars represent SEM. One- way ANOVA with Tukey's test was used for comparing means (**** p-value ≤0.0001). **(Ei, ii)** Representative images of alkaline and neutral comet assay of mESCs cultured on PA gels (Insets show single comets) and quantitative analysis of olive tail moment ($n \geq 30$ cells per condition across N = 3 independent experiments). One- way ANOVA with Tukey's test was used for comparing means (*p-value ≤0.05, ** p-value ≤0.01, ns = non-significant p-value>0.05). For all blots, GAPDH served as loading control

See also Figure S1 A-C.

Figure 2

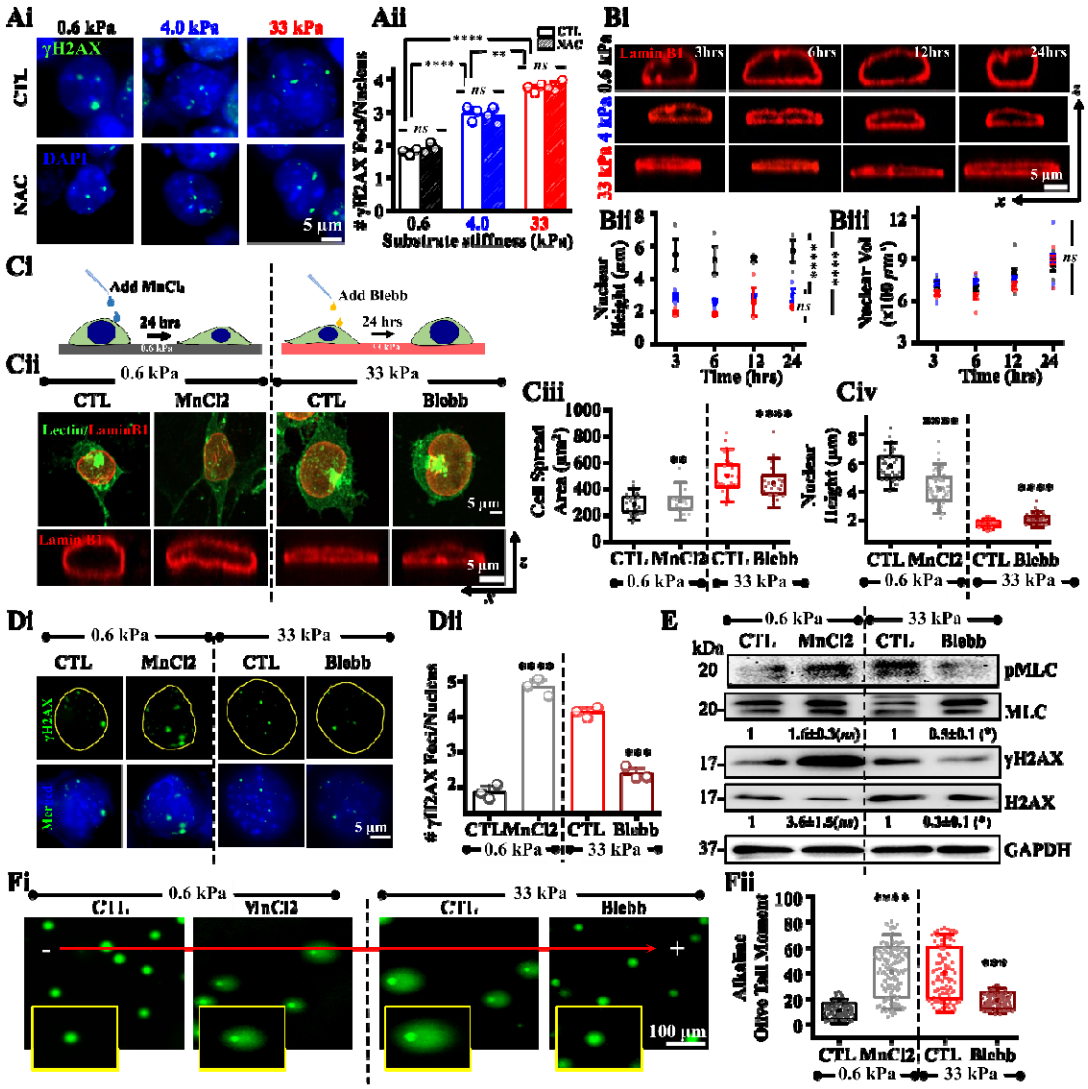

Figure 2: Mechanoadaptation mediated nuclear compression induces DNA damage in mESCs: **(Ai, Aii)** Representative images of mESC nuclei co-stained with γH2AX on PA gels of varying stiffnesses after 24 hrs in culture in presence and absence of the ROS inhibitor, N-acetyl cysteine (NAC) and quantification of DNA damage (cells per condition across N = 3 independent experiments). Scale Bar = 5μm. Error bars represent SEM. Two-way ANOVA followed by Tukey's post-hoc test was used to compare means (** -value 0.01, **** -value 0.0001, *ns* = non-significant -value 0.05). **(Bi-Biii)** Representative images showing transverse sections of mESC nuclei immunostained with Lamin B1 on PA gels of varying stiffness post 3, 6, 12 and 24 hours of seeding and quantification of nuclear height and nuclear volume (cells per condition across N = 3 independent experiments). Scale Bar = 5μm. Error bars represent SD. Two- way ANOVA with Tukey's test was used for comparing means (**** -value 0.0001, *ns* = non-significant p-value 0.05). **(Ci-Civ)** Schematic workflow, representative lectin-stained images and transverse Lamin B1 stained nuclear sections of mESCs on PA gels of 0.6 kPa +/- $MnCl_2$ and 33 kPa +/- Blebbistatin and quantification of cell spreading and nuclear height (cells per condition across N = 3 independent experiments). Scale Bar = 5μm. Error bars represent SD. Unpaired Student's t-test

was used for comparing means between control and treated samples on each PA gel (**p-value ≤0.01, **** p-value≤ 0.0001). **(Di, Dii)** γH2AX and DAPI immunostained images of mESCs on PA gels of 0.6 kPa +/- $MnCl_2$ and 33 kPa +/- Blebbistatin. Quantification of γH2AX foci (n ≥ 40 cells per condition across N = 3 independent experiments). Scale Bar = 5μm. Error bars represent SEM. Unpaired student t-test was used for comparing means between control and treated samples on each PA gel (***p-value ≤0.001, **** p-value≤ 0.0001). **(E)** Representative immunoblots and quantification of mean ±SEM of pMLC/MLC and γH2AX/H2AX levels in mESCs cultured on 0.6 kPa gels +/- $MnCl_2$ and 33 kPa gels +/- Blebbistatin (N = 3 independent experiments). Unpaired Student t-test was used for comparing means with respect to untreated controls of each PA gel (*p-value ≤0.05, *ns* = non-significant p-value>0.05). **(Fi, Fii)** Representative images of alkaline comet assay of mESCs cultured on 0.6 kPa +/- $MnCl_2$ and 33 kPa +/- Blebbistatin (Insets show single comets), and quantitative analysis of olive tail moment (n ≥ 30 cells per condition across N = 3 independent experiments). Scale Bar = 100 µm. Error bars represent SD. Unpaired Student's t-test was used for comparing means with respect to untreated controls of each PA gel (***p-value ≤0.001, **** p-value ≤0.0001). For all blots, GAPDH served as loading control.

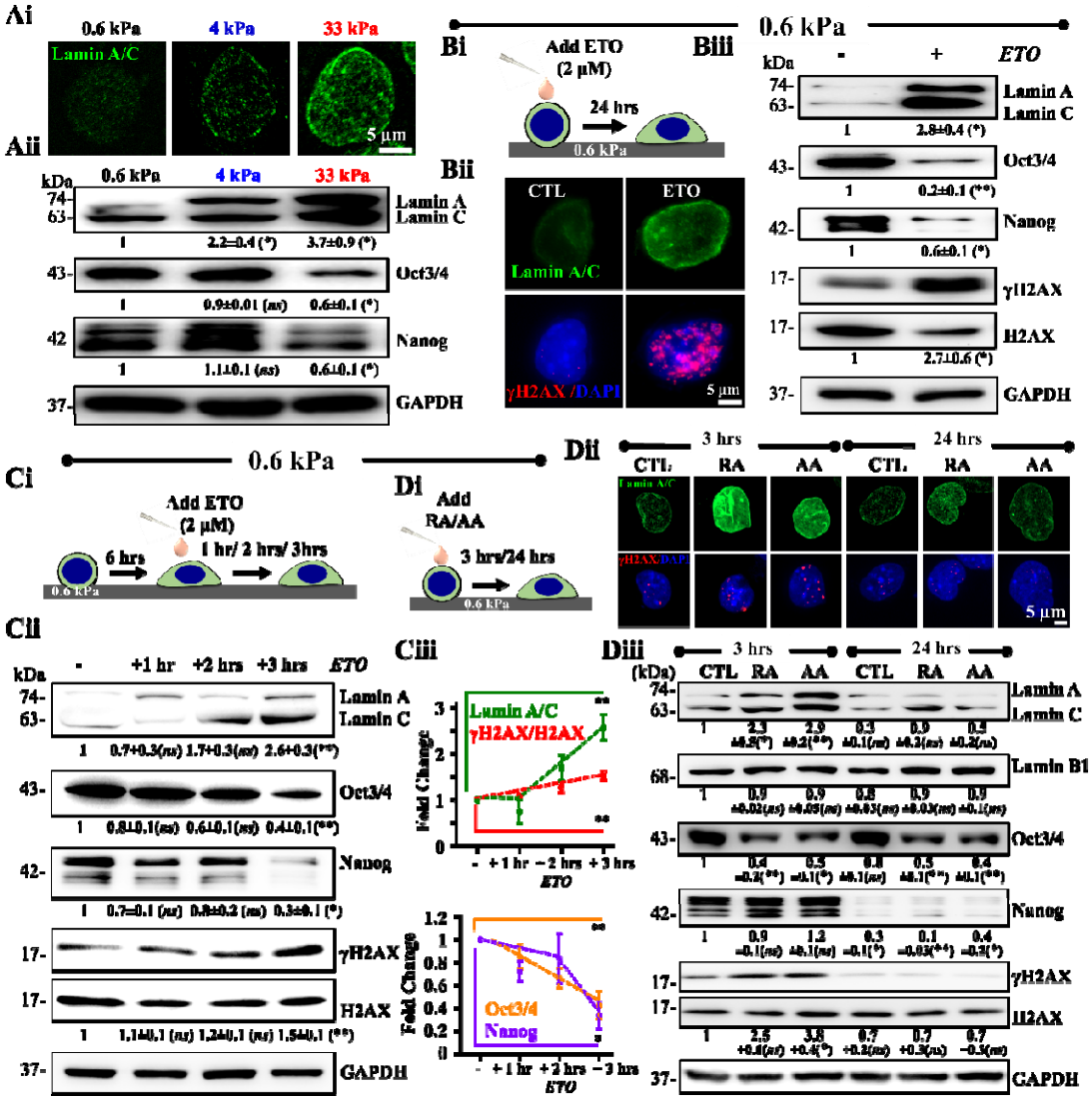

Figure 3

Figure 3: DNA damage induces Lamin A/C expression: (Ai, Aii) Representative images of mESC nuclei immunostained with Lamin A/C on PA gels of varying stiffnesses post 24 hrs of culture. Scale Bar = 5μm. Representative immunoblots and quantification of mean ±SEM of Lamin A/C expression and pluripotency (Oct3/4 and Nanog) of mESCs on varying stiffnesses post 24 hrs culture (N = 3 independent experiments). Two- way ANOVA with Tukey's test was used for comparing means with respect to 0.6 kPa conditions (* -value 0.05, *ns* = non-significant -value 0.05). **(Bi, Bii, Biii)** Experimental setup and representative images of Lamin A/C expression and DNA damage in presence of 2µM etoposide (ETO) post 24 hrs treatment on mESCs by immunofluorescence on 0.6 kPa gels. Scale Bar = 5μm. Representative immunoblots and quantification of mean ±SEM of Lamin A/C expression, pluripotency levels and γH2AX/H2AX of whole cell mESC lysates in presence and absence of ETO post 24 hrs treatment on 0.6 kPa gels (independent experiments). Unpaired student's t-test was used for comparing means with respect to untreated control. (* -value 0.05, ** -value 0.01). **(Ci, Cii, Ciii)** Experimental setup for studying temporal correlation between DNA damage and Lamin A/C induction. Cells were allowed to attach onto 0.6 kPa gels for 6 hrs prior to

ETO addition, and then cultured for upto 3 hrs. Representative immunoblots and quantification of mean ±SEM showing temporal evolution of Lamin A/C, Oct3/4, Nanog, γH2AX/H2AX ($N = 3$ independent experiments). One- way ANOVA with Tukey's test was used for comparing means with respect to untreated controls (*p-value ≤0.05, **p-value ≤0.01, *ns* = non-significant p-value>0.05). **(Di, Dii, Diii)** Schematic workflow and representative immunofluorescence images of Lamin A/C and γH2AX on mESCs post 3 hrs and 24 hrs of retinoic acid (RA) and ascorbic acid (AA) treatment on 0.6 kPa PA gels. Scale Bar = 5μm. Representative immunoblots and quantification of mean ±SEM of Lamin A/C, Lamin B1, Oct3/4, Nanog and γH2AX/H2AX of whole cell mESC lysates post treatment of RA and AA on 0.6 kPa PA gels ($N = 3$ independent experiments). Two- way ANOVA with Tukey's test was used for comparing means with respect to 3 hr CTL conditions (*p-value ≤0.05, **p-value ≤0.01, *ns* = non-significant p-value>0.05). For all blots, GAPDH served as loading control.
See also Figure S 1 Di, ii and Figure S 2 A, B.

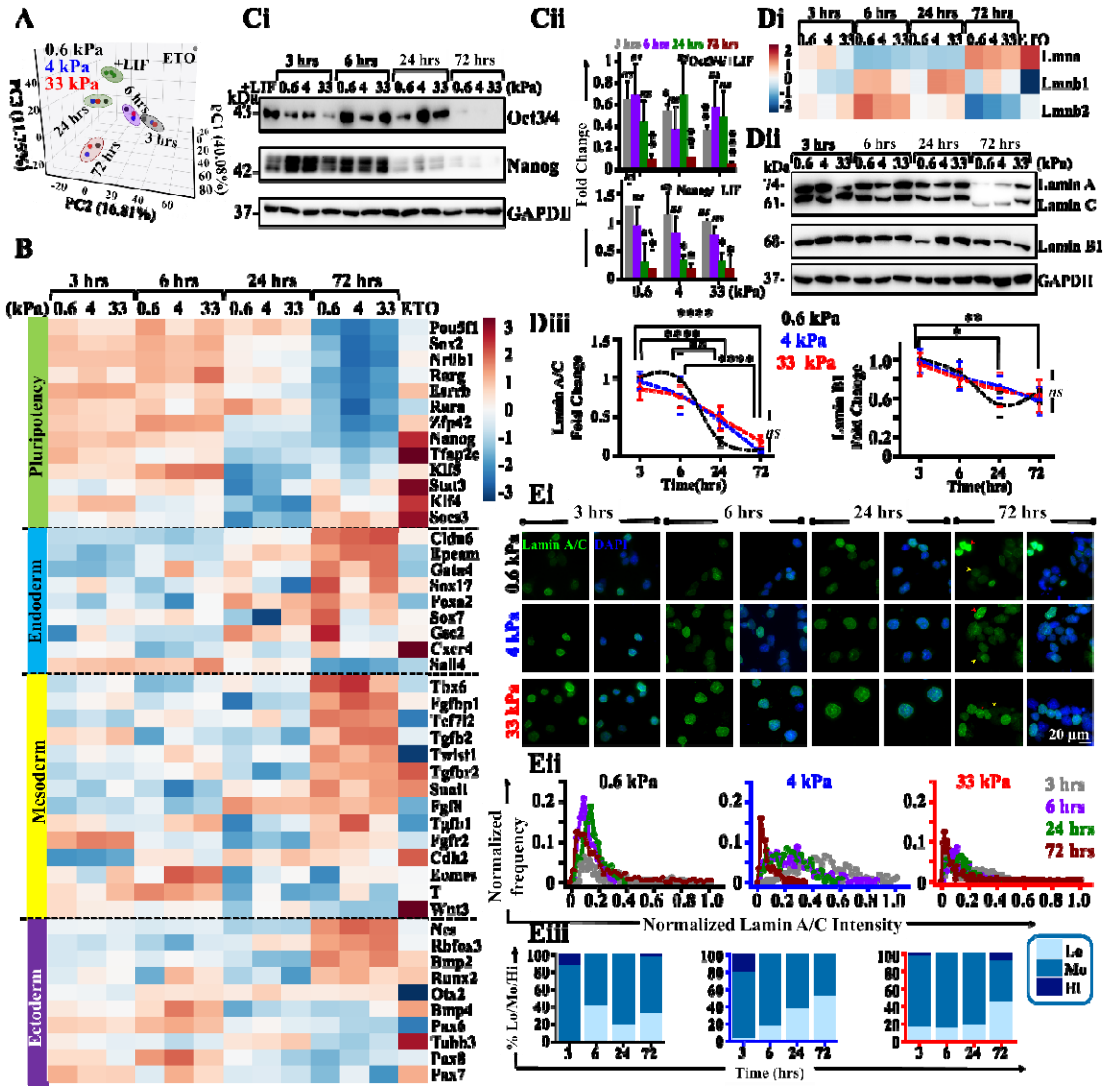

Figure 4

Figure 4: Germ layer differentiation is associated with loss in Lamin A/C: (A) 3-D PCA plot representing clusters of mESCs in +LIF condition, Etoposide (ETO) and varying stiffness post 3 hrs, 6 hrs, 24 hrs and 72 hrs of culture based on RNAseq profiles. **(B)** Heatmaps showing temporal evolution of mESC RNAseq profiles of genes involved in pluripotency, endodermal, mesodermal and ectodermal lineage across different stiffnesses and in ETO-treated cells on 0.6 kPa gels. Normalization was carried out with respect to +LIF condition. **(Ci, Cii)** Representative immunoblots and quantification of Oct3/4 and Nanog in mESCs cultured in the presence of LIF and in the absence of LIF on PA gels across different time-points (independent experiments; error bars represent SEM). Two- way ANOVA with Tukey's test was used for comparing means with respect to +LIF controls (* -value 0.05, ** -value 0.01, *** -value 0.001, ns = non-significant *p*-value 0.05). **(Di)** Heatmaps showing RNAseq profiles of Lamin genes (*LMNA, LMNB1 and LMNB2*) in mESCs cultured on PA gels across different time-points as well as in ETO treated cells on 0.6 kPa gels. Normalization was carried out with respect to +LIF condition. **(Dii, Diii)** Representative immunoblots and quantification of Lamin A/C and Lamin B1 in mESCs cultured on PA gels across different time-points (independent experiments; error bars represent ±SEM). Quantification of Lamin A/C

and Lamin B1 levels were normalized with respect to 0.6 kPa at 3 hrs at different timepoints on the gels. Statistical significance obtained by Two-way ANOVA followed by Tukey's tests (*p-value ≤0.05, **p-value ≤0.01, ****p-value ≤0.0001, *ns* = non-significant p-value >0.05). **(Ei-Eiii)** Representative immunofluorescence images of Lamin A/C co-stained with DAPI in mESCs cultured on PA gels across different time-points showing heterogenous expression of Lamin A/C (red arrowhead: high expression; yellow arrowhead: low expression) ($n \geq 50$ cells per condition across N = 3 independent experiments). Scale Bar = $20\mu m$. Lamin A/C heterogeneity was captured by plotting the normalized Lamin A/C distribution across different time-points. Normalization was done wrt the maximum intensity observed across all conditions and timepoints ($n \geq 50$ cells per condition across N = 3 independent experiments). Assessment of percentage of low (Lo), moderate (Mo) and high (Hi) Lamin A/C expression across different conditions (see Materials & Methods for details). For all blots, GAPDH served as loading control.
See also Figure S 3- S 5.

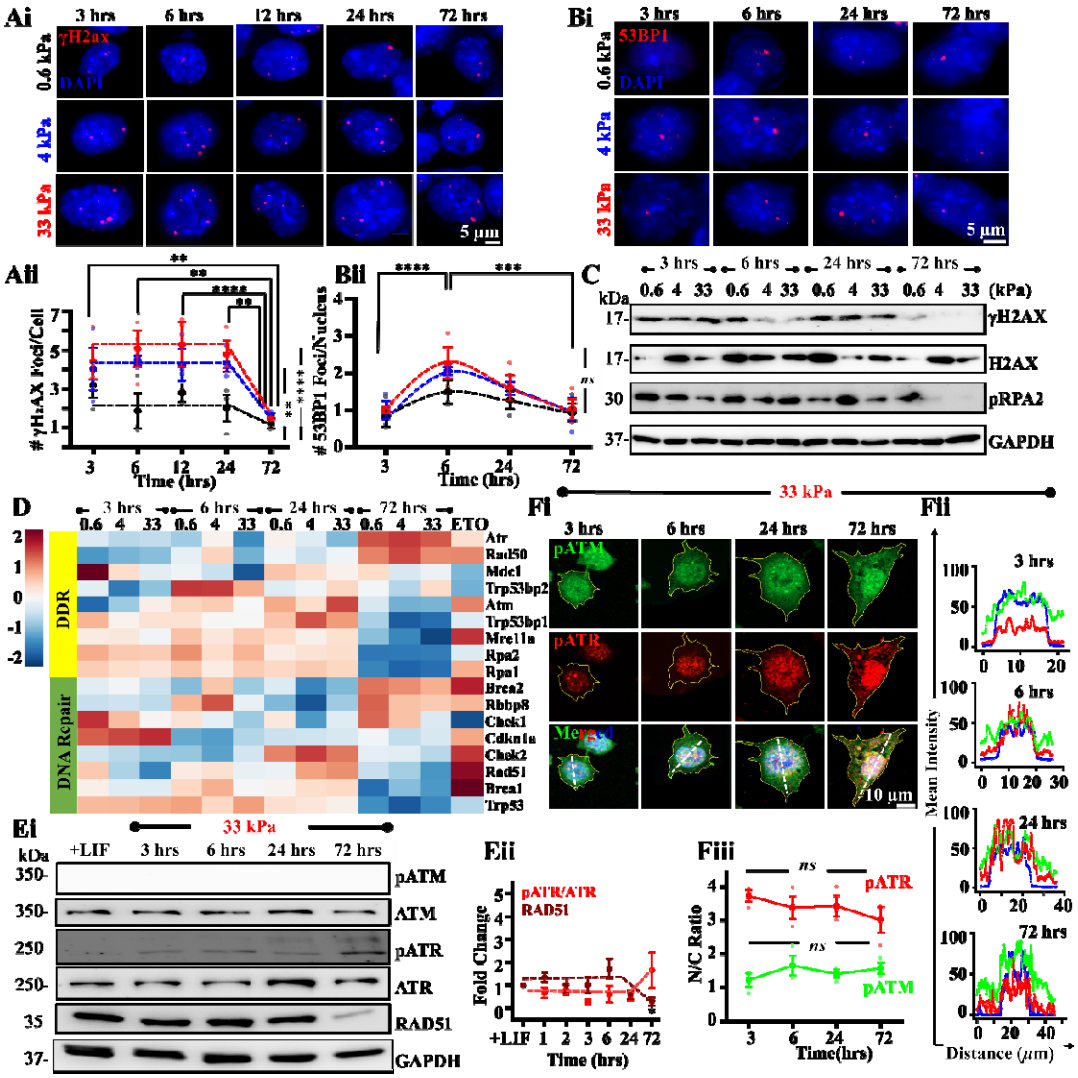

Figure 5

Figure 5: Differentiation involves DNA repair through ATR activation and nuclear enrichment: (Ai, Aii) Representative images of temporal evolution of mESCs immunostained for γH2AX co-stained with DAPI on varying stiffness and quantification of γH2AX foci count per nucleus (cells per condition across N = 3 independent experiments). Scale Bar = 5μm. Error bars represent SD. Two- way ANOVA with Tukey's test was used for comparing means (** -value 0.01, **** -value 0.0001). **(Bi, Bii)** Representative images of temporal evolution of mESCs immunostained for DDR factor, 53BP1, co-stained with DAPI on varying stiffness and quantification of 53BP1 foci count per nucleus (cells per condition across N = 3 independent experiments). Scale Bar = 5μm. Error bars represent SD. Two- way ANOVA with Tukey's test was used for comparing means (*** p-value 0.001, **** -value 0.0001, *ns* = non-significant -value 0.05). **(C)** Immunoblots representing temporal expression of DDR factors, γH2AX/H2AX and pRPA2 of mESCs on varying stiffness. **(D)** Heatmaps showing temporal evolution of mESC RNAseq profiles of genes involved in DNA damage response (DDR) factors and DNA repair across different stiffnesses and in ETO-treated cells on 0.6 kPa gels. Normalization was carried out with respect to +LIF condition. **(Ei, Eii)** Immunoblots representing temporal expression of DDR factors (pATM/ATM, pATR/ATR) and DNA repair factor (RAD 51) in the presence of LIF and in the absence of LIF on 33

kPa PA gels. Quantification of pATR/ATR, ATR, ATM and RAD51 levels were done with respect to +LIF condition at different timepoints across N = 3 independent experiments. Error bars represent ±SEM. One- way ANOVA with Tukey's test was used for comparing means (*p-value ≤0.05). **(Fi, ii)** Representative pATM-Ser1981/pATR-Thr1989/DAPI stained images of mESCs across different timepoints on 33 kPa gels. Scale Bar = 5μm**.** Representative intensity profiles along white dotted lines depict nuclear/cytoplasmic localization of pATM (green) and pATR (red). **(Fiii)** Quantification of nuclear to cytoplasmic (N/C) ratio of pATM (green) and pATR (red) ($n \geq 50$ cells per condition across N = 3 independent experiments). Error bars represent SD. One- way ANOVA with Tukey's test was used for comparing means (*ns* = non-significant p-value>0.05). For all blots, GAPDH served as loading control.
See also Figure S 6 A-D and Movies S 1-3.

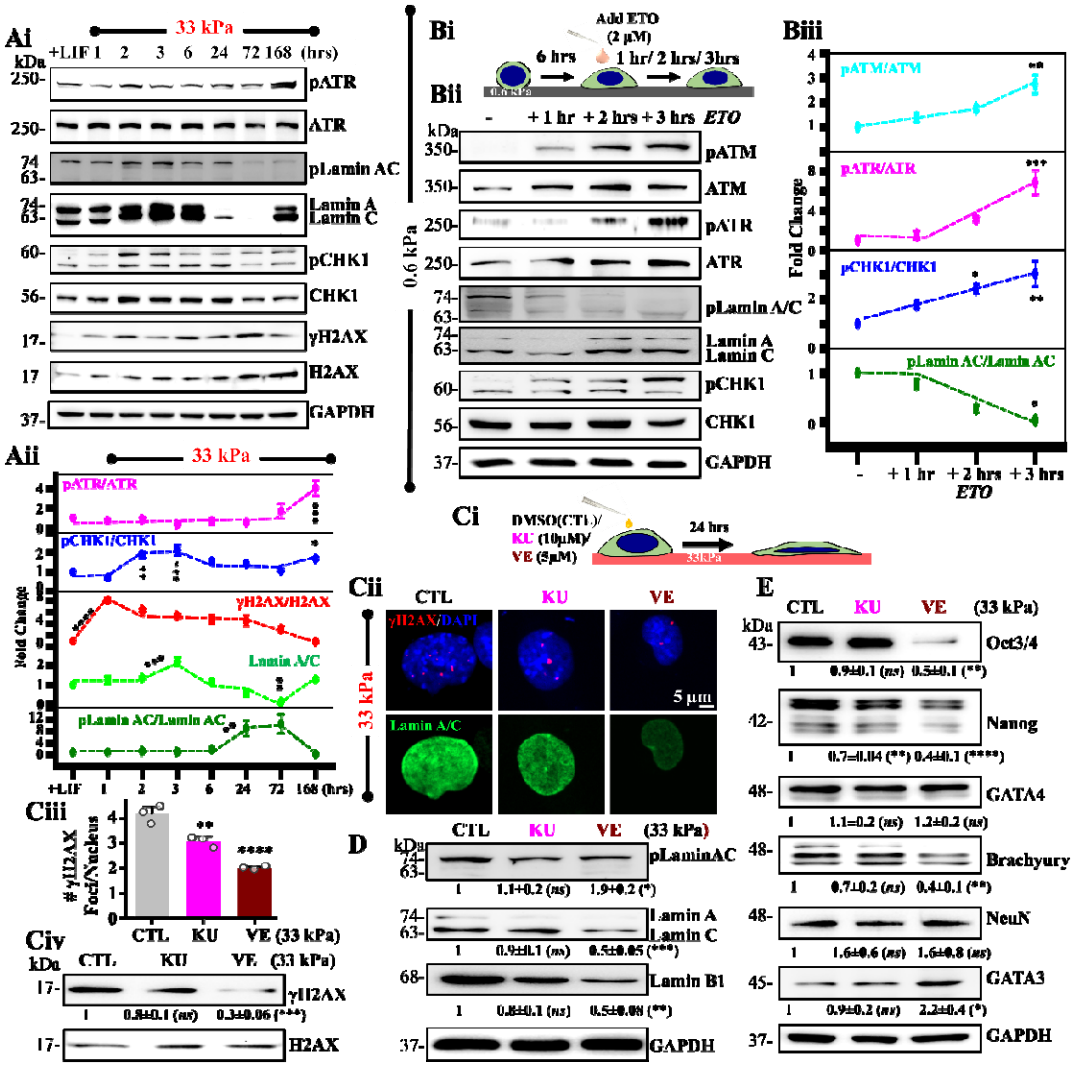

Figure 6

Figure 6: ATR regulates Lamin expression: (Ai, Aii) Immunoblots representing temporal evolution of pATR/ATR, pLamin A/C/Lamin A/C, pCHK1/CHK1, γH2AX/H2AX in the presence of LIF and in the absence of LIF on 33 kPa PA gels upto Day 7 (168 hrs). Quantification of mean ±SEM of pATR/ATR, pCHK1/CHK1, γH2AX/H2AX, Lamin A/C and pLamin A/C/Lamin A/C normalized with respect to +LIF condition (independent experiments). One- way ANOVA with Tukey's test was used for comparing means with respect to +LIF controls (* -value 0.05, ** -value 0.01, *** -value 0.001, **** -value 0.0001). **(Bi, ii, iii)** Cells were allowed to attach onto 0.6 kPa gels for 6 hrs prior to ETO addition, and then cultured for upto 3 hrs. Representative immunoblots showing temporal evolution of pATM/ATM, pATR/ATR and pCHK1/CHK1, and its quantification of mean SEM (independent experiments). One- way ANOVA with Tukey's test was used for comparing means with respect to untreated controls (* -value 0.05, ** -value 0.01, *** -value 0.001). **(Ci-iv)** Experimental setup for studying effect of KU-55933 (KU) and VE-821 (VE) on Lamin A/C. Cells were cultured on 33 kPa gels for 24 hrs. Representative immunostained images of γH2AX co-stained with DAPI and Lamin A/C on mESCs cultured in the presence and absence of KU and VE. Bar plots show quantification of γH2AX foci per nucleus in these conditions (cells per condition across N = 3 independent experiments). Scale Bar = 5μm. Error bars represent SEM.

Unpaired student t-test was used for comparing means between control and treated samples (**p-value ≤0.01, ****p-value ≤0.0001). Representative immunoblots showing quantification of mean ±SEM of γH2AX/H2AX (N = 3 independent experiments). One- way ANOVA with Tukey's test was used for comparing means with respect to untreated control (***p -value ≤0.001, *ns* = non-significant p-value>0.05). **(D)** Representative immunoblots of mESCs on 33 kPa gels in the presence and absence of KU and VE and quantification of mean ±SEM showing pLamin A/C/Lamin A/C, Lamin A/C and Lamin B1 expression ($N = 3$ independent experiments). One- way ANOVA with Tukey's test was used for comparing means with respect to untreated controls (*p-value ≤0.05, **p-value ≤0.01, ***p-value ≤0.001, *ns* = non-significant). **(E)** Representative immunoblots of mESCs on 33 kPa gels in the presence and absence of KU and VE and quantification of mean ±SEM showing Oct3/4, Nanog, GATA4, Brachyury, NeuN and GATA3 expression ($N = 3$ independent experiments). One- way ANOVA with Tukey's test was used for comparing means with respect to untreated control (*p-value ≤0.05, **p-value ≤0.01, ****p-value ≤0.0001, ns = non-significant). For all blots, GAPDH served as loading control.
See also Figure S 7.

Figure 7:

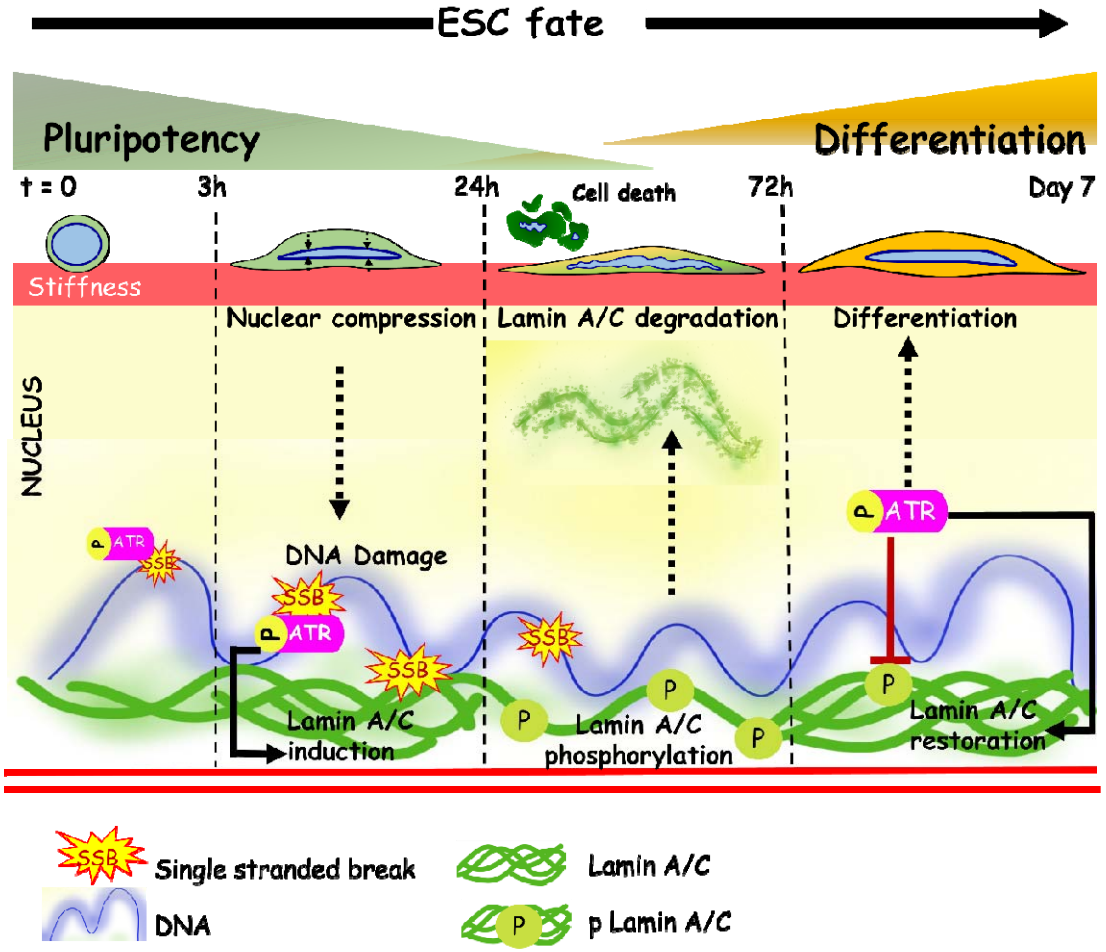

Figure 7: Schematic representation depicting stiffness-dependent differentiation in mouse ESCs. Stiffness-dependent mechanoadaptation induces nuclear compression leading to DNA damage (SSBs), activation of ATR and ATR-mediated lamin A/C modulation. Differentiation involves ATR-mediated lamin A/C stabilization by inhibition of Lamin A/C phosphorylation at early time-points followed by gradual loss of Lamin A/C and cell death. ATR activation in surviving cells at later timepoints restores Lamin A/C.

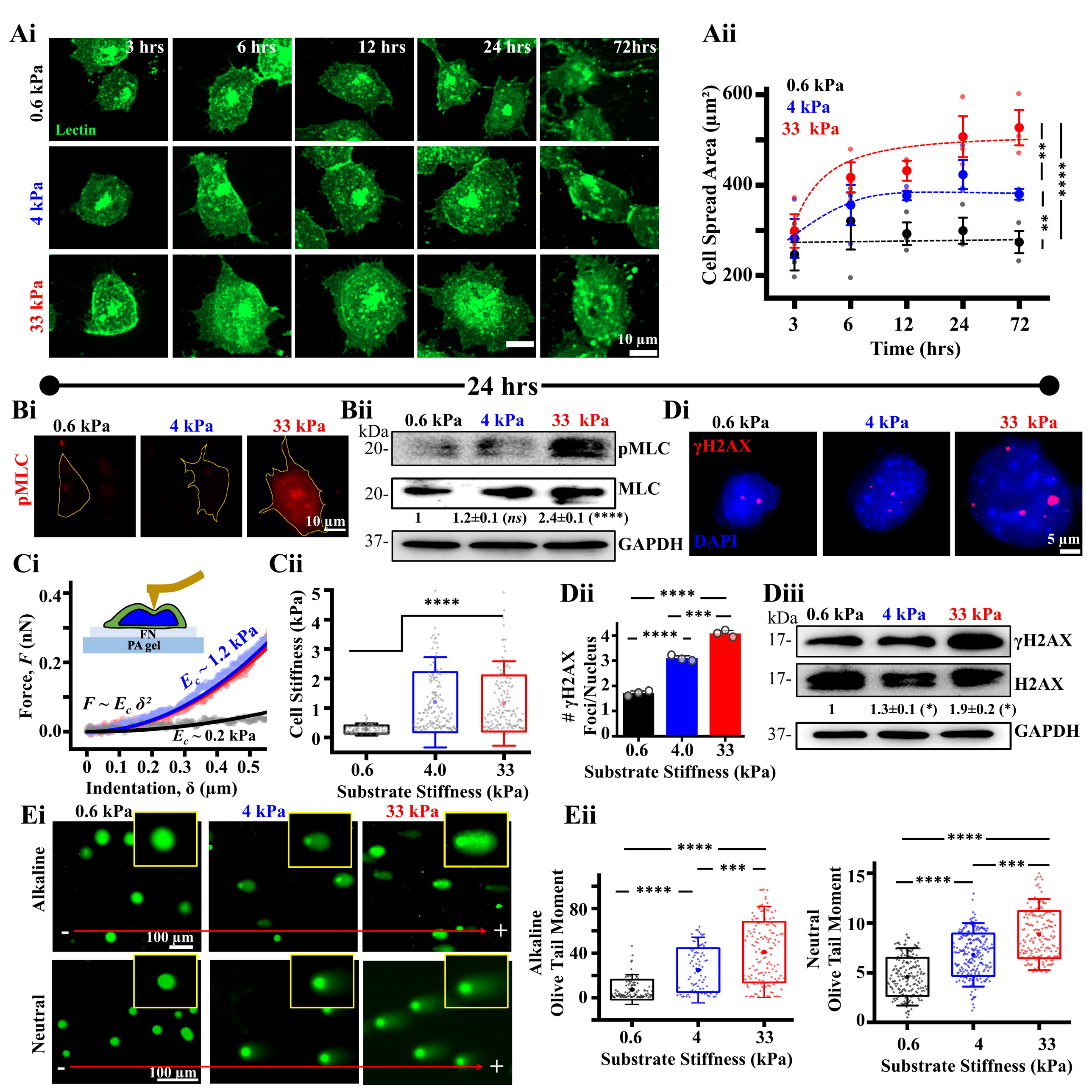
Ai
3 hrs
6 hrs
12 hrs
24 hrs
72hrs
0.6 kPa
4 kPa
33 kPa
Lectin
10 µm
Aii
0.6 kPa
4 kPa
33 kPa
Cell Spread Area (µm²)
600
400
200
3
6
12
24
72
Time (hrs)
**
**
****
24 hrs
Bi
0.6 kPa
4 kPa
33 kPa
pMLC
10 µm
Bii
kDa
0.6 kPa
4 kPa
33 kPa
20-
pMLC
20-
MLC
1
1.2±0.1 (ns)
2.4±0.1 (****)
37-
GAPDH
Di
0.6 kPa
4 kPa
33 kPa
γH2AX
DAPI
5 µm
Ci
FN
PA gel
Force, F (nN)
0.4
0.2
0.0
E_c ~ 1.2 kPa
F ~ E_c δ²
E_c ~ 0.2 kPa
0
0.1
0.2
0.3
0.4
0.5
Indentation, δ (µm)
Cii
Cell Stiffness (kPa)
5
4
3
2
1
0
****
0.6
4.0
33
Substrate Stiffness (kPa)
Dii
****
***
****
γH2AX Foci/Nucleus
4
3
2
1
0
0.6
4.0
33
Substrate Stiffness (kPa)
Diii
kDa
0.6 kPa
4 kPa
33 kPa
17-
γH2AX
17-
H2AX
1
1.3±0.1 (*)
1.9±0.2 (*)
37-
GAPDH
Ei
0.6 kPa
4 kPa
33 kPa
Alkaline
Neutral
-
+
100 µm
Eii
****
***
****
Alkaline Olive Tail Moment
80
40
0
0.6
4
33
Substrate Stiffness (kPa)
****
***
****
Neutral Olive Tail Moment
15
10
5
0
0.6
4
33
Substrate Stiffness (kPa)

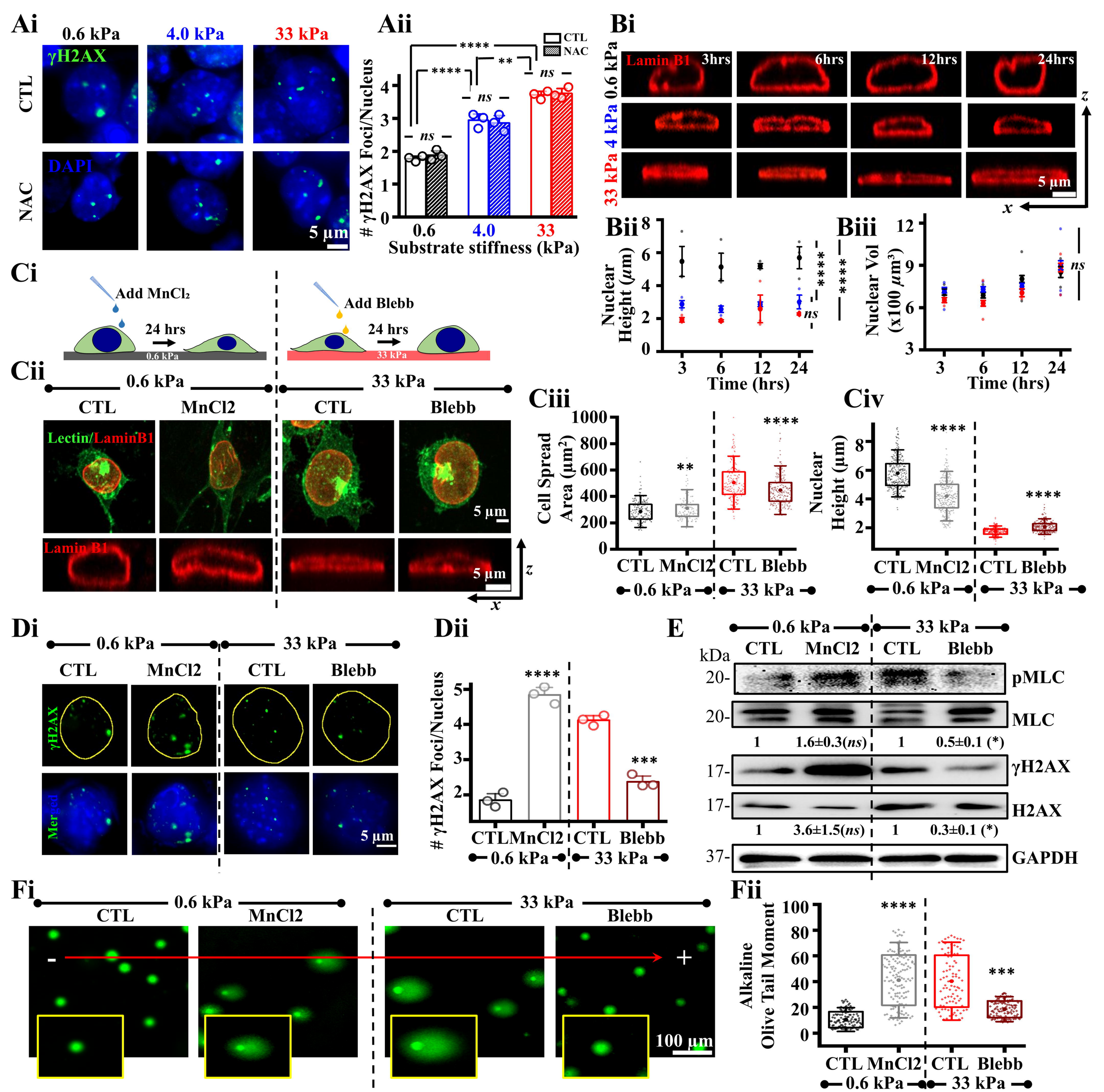
Ai
0.6 kPa
4.0 kPa
33 kPa
CTL
NAC
γH2AX
DAPI
5 µm
Aii
CTL
NAC
γH2AX Foci/Nucleus
Substrate stiffness (kPa)
0.6
4.0
33
ns
****
**
Bi
Lamin B1
3hrs
6hrs
12hrs
24hrs
0.6 kPa
4 kPa
33 kPa
5 µm
z
x
Bii
Nuclear Height (µm)
Time (hrs)
Biii
Nuclear Vol (x100 µm³)
Time (hrs)
Ci
Add MnCl₂
24 hrs
0.6 kPa
Add Blebb
24 hrs
33 kPa
Cii
0.6 kPa
33 kPa
CTL
MnCl2
CTL
Blebb
Lectin/LaminB1
Lamin B1
5 µm
Ciii
Cell Spread Area (µm²)
CTL MnCl2 CTL Blebb
0.6 kPa
33 kPa
Civ
Nuclear Height (µm)
CTL MnCl2 CTL Blebb
0.6 kPa
33 kPa
Di
0.6 kPa
33 kPa
CTL
MnCl2
CTL
Blebb
γH2AX
Merged
5 µm
Dii
γH2AX Foci/Nucleus
CTL MnCl2 CTL Blebb
0.6 kPa
33 kPa
E
0.6 kPa
33 kPa
kDa
CTL
MnCl2
CTL
Blebb
20-
pMLC
20-
MLC
1
1.6±0.3(ns)
1
0.5±0.1 (*)
17-
γH2AX
17-
H2AX
1
3.6±1.5(ns)
1
0.3±0.1 (*)
37-
GAPDH
Fi
0.6 kPa
33 kPa
CTL
MnCl2
CTL
Blebb
-
+
100 µm
Fii
Alkaline Olive Tail Moment
CTL MnCl2 CTL Blebb
0.6 kPa
33 kPa

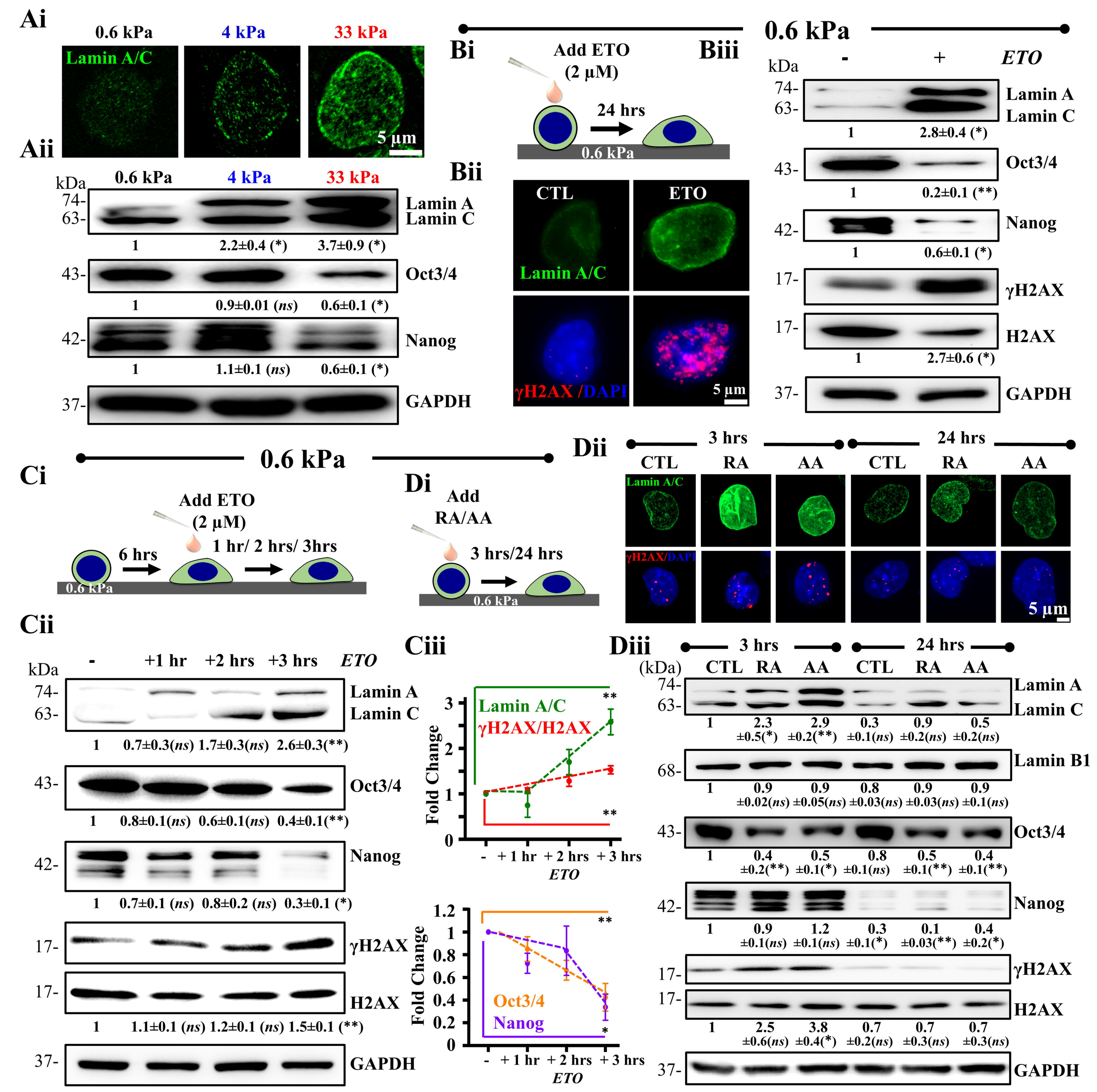
Ai
0.6 kPa
4 kPa
33 kPa
Lamin A/C
5 µm
Aii
kDa
0.6 kPa
4 kPa
33 kPa
74-
63-
Lamin A
Lamin C
1
2.2±0.4 (*)
3.7±0.9 (*)
43-
Oct3/4
1
0.9±0.01 (ns)
0.6±0.1 (*)
42-
Nanog
1
1.1±0.1 (ns)
0.6±0.1 (*)
37-
GAPDH
Bi
Add ETO
(2 µM)
24 hrs
0.6 kPa
Bii
CTL
ETO
Lamin A/C
γH2AX /DAPI
5 µm
Biii
0.6 kPa
kDa
-
+
ETO
74-
63-
Lamin A
Lamin C
1
2.8±0.4 (*)
43-
Oct3/4
1
0.2±0.1 (**)
42-
Nanog
1
0.6±0.1 (*)
17-
γH2AX
17-
H2AX
1
2.7±0.6 (*)
37-
GAPDH
Ci
0.6 kPa
Add ETO
(2 µM)
6 hrs
1 hr/ 2 hrs/ 3hrs
0.6 kPa
Di
Add
RA/AA
3 hrs/24 hrs
0.6 kPa
Dii
3 hrs
24 hrs
CTL
RA
AA
CTL
RA
AA
Lamin A/C
γH2AX/DAPI
5 µm
Cii
kDa
-
+1 hr
+2 hrs
+3 hrs
ETO
74-
63-
Lamin A
Lamin C
1
0.7±0.3(ns)
1.7±0.3(ns)
2.6±0.3(**)
43-
Oct3/4
1
0.8±0.1(ns)
0.6±0.1(ns)
0.4±0.1(**)
42-
Nanog
1
0.7±0.1 (ns)
0.8±0.2 (ns)
0.3±0.1 (*)
17-
γH2AX
17-
H2AX
1
1.1±0.1 (ns)
1.2±0.1 (ns)
1.5±0.1 (**)
37-
GAPDH
Ciii
Lamin A/C
γH2AX/H2AX
Fold Change
0
1
2
3
**
**
-
+ 1 hr
+ 2 hrs
+ 3 hrs
ETO
Oct3/4
Nanog
Fold Change
0
0.2
0.4
0.6
0.8
1
1.2
**
*
-
+ 1 hr
+ 2 hrs
+ 3 hrs
ETO
Diii
3 hrs
24 hrs
(kDa)
CTL
RA
AA
CTL
RA
AA
74-
63-
Lamin A
Lamin C
1
2.3 ±0.5(*)
2.9 ±0.2(**)
0.3 ±0.1(ns)
0.9 ±0.2(ns)
0.5 ±0.2(ns)
68-
Lamin B1
1
0.9 ±0.02(ns)
0.9 ±0.05(ns)
0.8 ±0.03(ns)
0.9 ±0.03(ns)
0.9 ±0.1(ns)
43-
Oct3/4
1
0.4 ±0.2(**)
0.5 ±0.1(*)
0.8 ±0.1(ns)
0.5 ±0.1(**)
0.4 ±0.1(**)
42-
Nanog
1
0.9 ±0.1(ns)
1.2 ±0.1(ns)
0.3 ±0.1(*)
0.1 ±0.03(**)
0.4 ±0.2(*)
17-
γH2AX
17-
H2AX
1
2.5 ±0.6(ns)
3.8 ±0.4(*)
0.7 ±0.2(ns)
0.7 ±0.3(ns)
0.7 ±0.3(ns)
37-
GAPDH

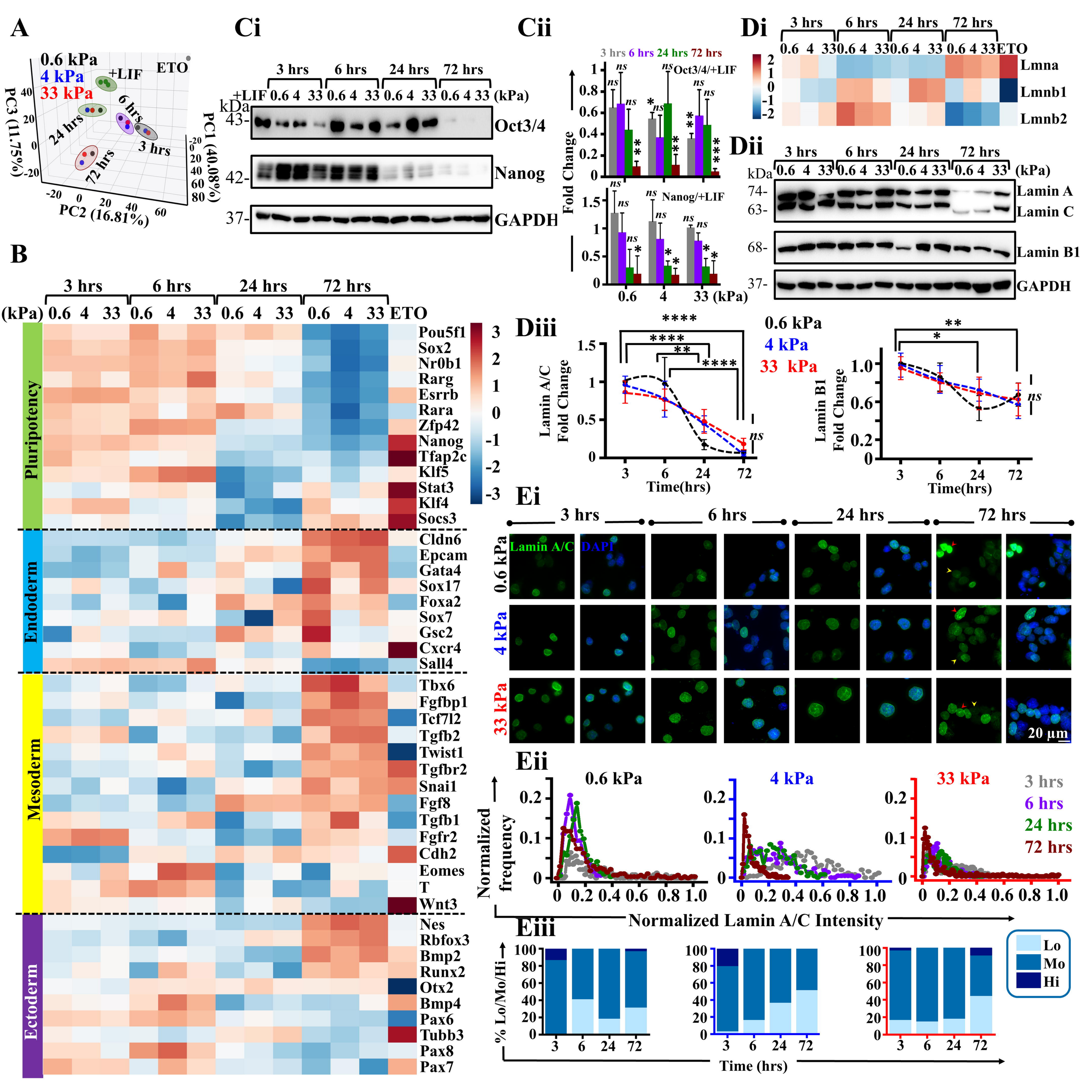
A
0.6 kPa
4 kPa
33 kPa
+LIF
ETO
6 hrs
24 hrs
3 hrs
72 hrs
PC3 (11.75%)
PC2 (16.81%)
PC1 (40.08%)
Ci
3 hrs
6 hrs
24 hrs
72 hrs
+LIF 0.6 4 33 0.6 4 33 0.6 4 33 0.6 4 33 (kPa)
kDa
43-
42-
37-
Oct3/4
Nanog
GAPDH
Cii
3 hrs 6 hrs 24 hrs 72 hrs
Oct3/4/+LIF
Nanog/+LIF
Fold Change
0.6
4
33 (kPa)
Di
3 hrs
6 hrs
24 hrs
72 hrs
0.6 4 33 0.6 4 33 0.6 4 33 0.6 4 33 ETO
Lmna
Lmnb1
Lmnb2
Dii
3 hrs
6 hrs
24 hrs
72 hrs
kDa 0.6 4 33 0.6 4 33 0.6 4 33 0.6 4 33 (kPa)
74-
63-
68-
37-
Lamin A
Lamin C
Lamin B1
GAPDH
B
3 hrs
6 hrs
24 hrs
72 hrs
(kPa) 0.6 4 33 0.6 4 33 0.6 4 33 0.6 4 33 ETO
Pluripotency
Pou5f1
Sox2
Nr0b1
Rarg
Esrrb
Rara
Zfp42
Nanog
Tfap2c
Klf5
Stat3
Klf4
Socs3
Endoderm
Cldn6
Epcam
Gata4
Sox17
Foxa2
Sox7
Gsc2
Cxcr4
Sall4
Mesoderm
Tbx6
Fgfbp1
Tcf7l2
Tgfb2
Twist1
Tgfbr2
Snai1
Fgf8
Tgfb1
Fgfr2
Cdh2
Eomes
T
Wnt3
Ectoderm
Nes
Rbfox3
Bmp2
Runx2
Otx2
Bmp4
Pax6
Tubb3
Pax8
Pax7
Diii
0.6 kPa
4 kPa
33 kPa
Lamin A/C Fold Change
Lamin B1 Fold Change
Time(hrs)
Ei
3 hrs
6 hrs
24 hrs
72 hrs
Lamin A/C
DAPI
0.6 kPa
4 kPa
33 kPa
20 µm
Eii
0.6 kPa
4 kPa
33 kPa
3 hrs
6 hrs
24 hrs
72 hrs
Normalized frequency
Normalized Lamin A/C Intensity
Eiii
% Lo/Mo/Hi
Time (hrs)
Lo
Mo
Hi

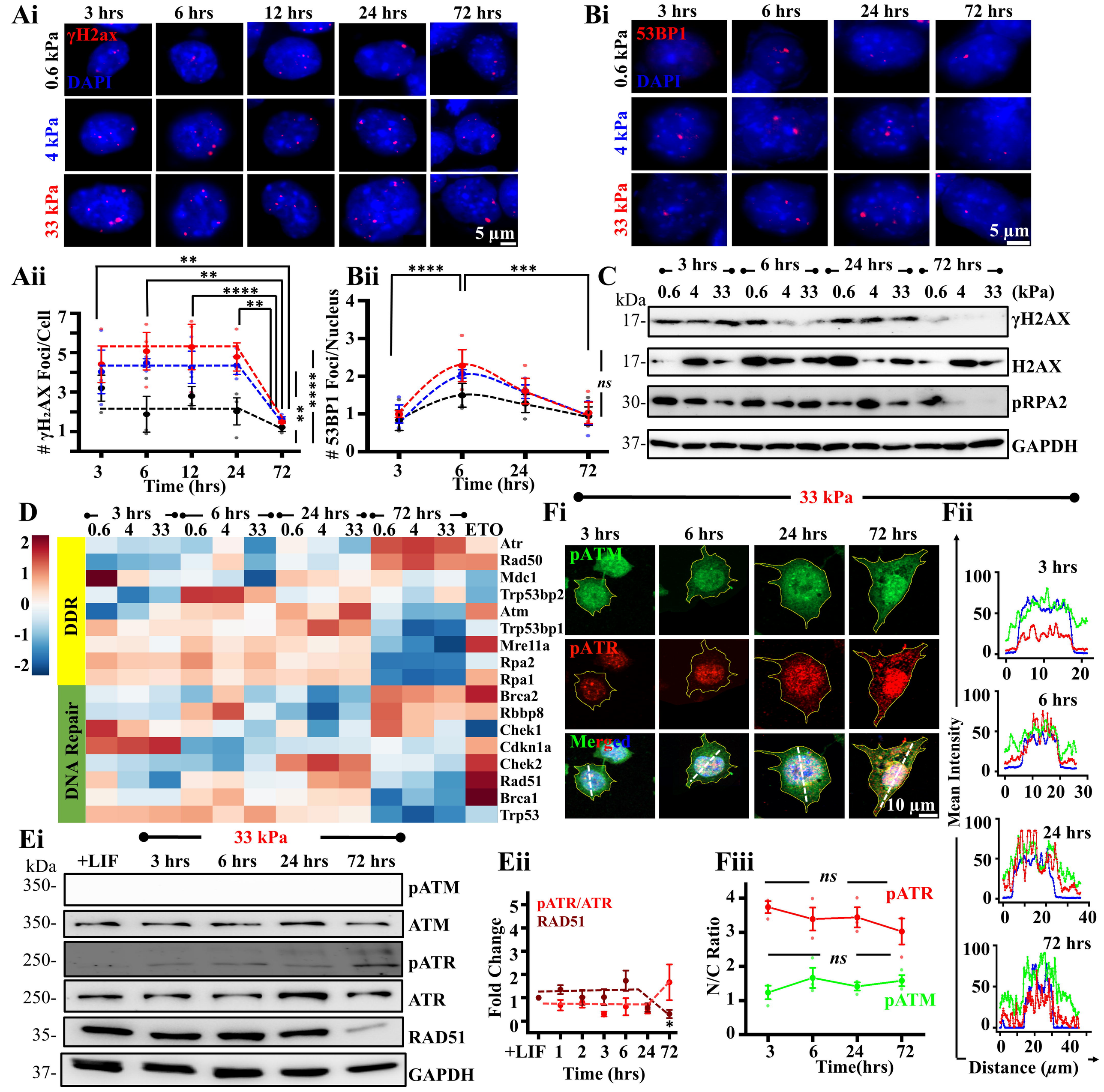
Ai
3 hrs
6 hrs
12 hrs
24 hrs
72 hrs
γH2ax
DAPI
0.6 kPa
4 kPa
33 kPa
5 µm
Bi
53BP1
DAPI
5 µm
Aii
γH2AX Foci/Cell
Time (hrs)
Bii
53BP1 Foci/Nucleus
ns
Time (hrs)
C
kDa
0.6 4 33 0.6 4 33 0.6 4 33 0.6 4 33 (kPa)
γH2AX
H2AX
pRPA2
GAPDH
D
0.6 4 33 0.6 4 33 0.6 4 33 0.6 4 33 ETO
DDR
DNA Repair
Atr
Rad50
Mdc1
Trp53bp2
Atm
Trp53bp1
Mre11a
Rpa2
Rpa1
Brca2
Rbbp8
Chek1
Cdkn1a
Chek2
Rad51
Brca1
Trp53
Fi
pATM
pATR
Merged
10 µm
Fii
Mean Intensity
Distance (µm)
Ei
kDa
+LIF
pATM
ATM
pATR
ATR
RAD51
GAPDH
Eii
pATR/ATR
RAD51
Fold Change
Time (hrs)
Fiii
ns
pATR
pATM
N/C Ratio
Time(hrs)

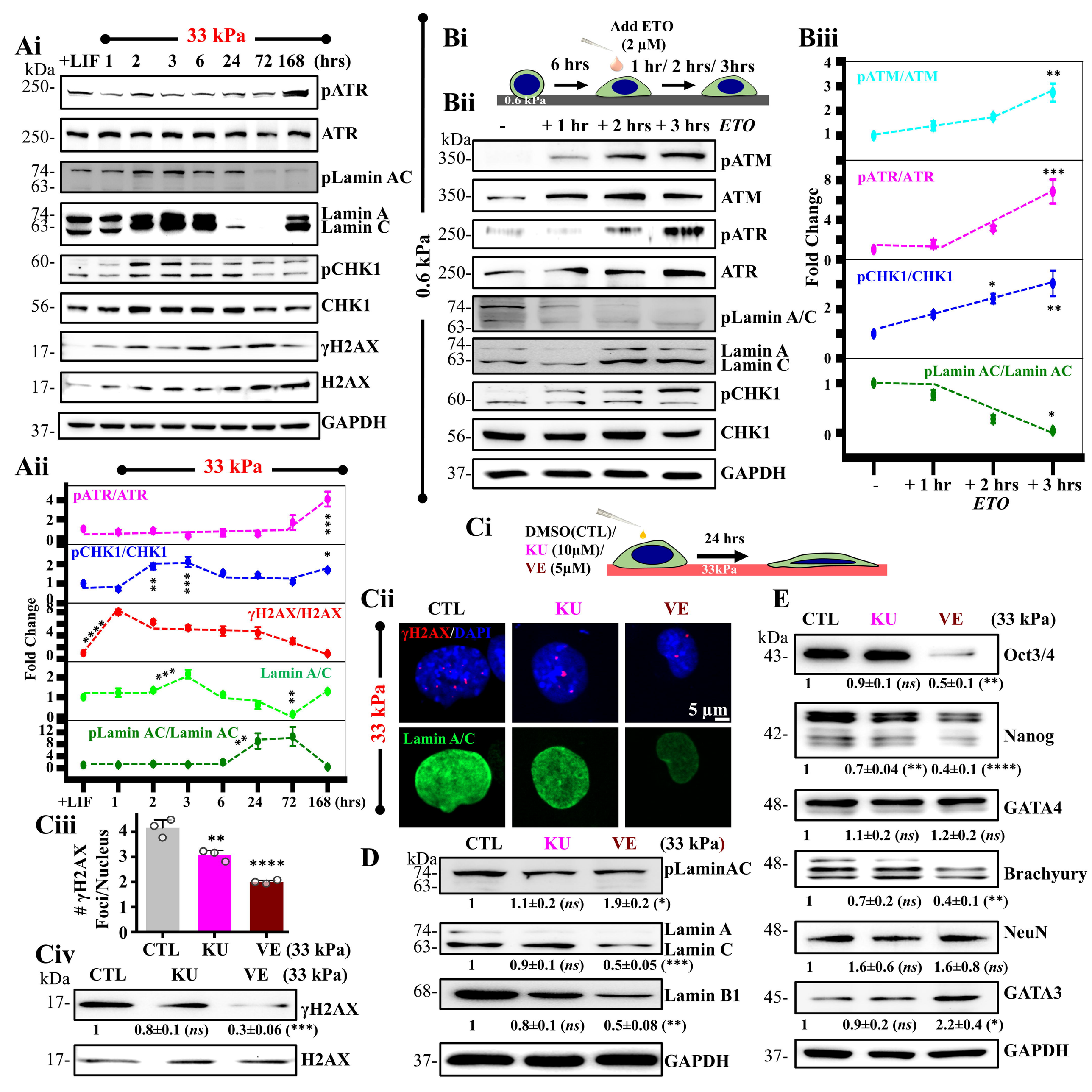
Ai
33 kPa
+LIF 1 2 3 6 24 72 168 (hrs)
kDa
250- pATR
250- ATR
74- 63- pLamin AC
74- 63- Lamin A Lamin C
60- pCHK1
56- CHK1
17- γH2AX
17- H2AX
37- GAPDH
Aii
33 kPa
pATR/ATR
pCHK1/CHK1
γH2AX/H2AX
Lamin A/C
pLamin AC/Lamin AC
Fold Change
+LIF 1 2 3 6 24 72 168 (hrs)
Bi
Add ETO (2 μM)
6 hrs
1 hr/ 2 hrs/ 3hrs
0.6 kPa
Bii
- + 1 hr + 2 hrs + 3 hrs ETO
kDa
350- pATM
350- ATM
250- pATR
250- ATR
74- 63- pLamin A/C
74- 63- Lamin A Lamin C
60- pCHK1
56- CHK1
37- GAPDH
0.6 kPa
Biii
pATM/ATM
pATR/ATR
pCHK1/CHK1
pLamin AC/Lamin AC
Fold Change
- + 1 hr + 2 hrs + 3 hrs
ETO
Ci
DMSO(CTL)/
KU (10μM)/
VE (5μM)
24 hrs
33kPa
Cii
CTL KU VE
γH2AX/DAPI
Lamin A/C
5 μm
33 kPa
Ciii
γH2AX Foci/Nucleus
CTL KU VE (33 kPa)
Civ
kDa
CTL KU VE (33 kPa)
17- γH2AX
1 0.8±0.1 (ns) 0.3±0.06 (***)
17- H2AX
D
CTL KU VE (33 kPa)
kDa
74- 63- pLaminAC
1 1.1±0.2 (ns) 1.9±0.2 (*)
74- 63- Lamin A Lamin C
1 0.9±0.1 (ns) 0.5±0.05 (***)
68- Lamin B1
1 0.8±0.1 (ns) 0.5±0.08 (**)
37- GAPDH
E
CTL KU VE (33 kPa)
kDa
43- Oct3/4
1 0.9±0.1 (ns) 0.5±0.1 (**)
42- Nanog
1 0.7±0.04 (**) 0.4±0.1 (****)
48- GATA4
1 1.1±0.2 (ns) 1.2±0.2 (ns)
48- Brachyury
1 0.7±0.2 (ns) 0.4±0.1 (**)
48- NeuN
1 1.6±0.6 (ns) 1.6±0.8 (ns)
45- GATA3
1 0.9±0.2 (ns) 2.2±0.4 (*)
37- GAPDH

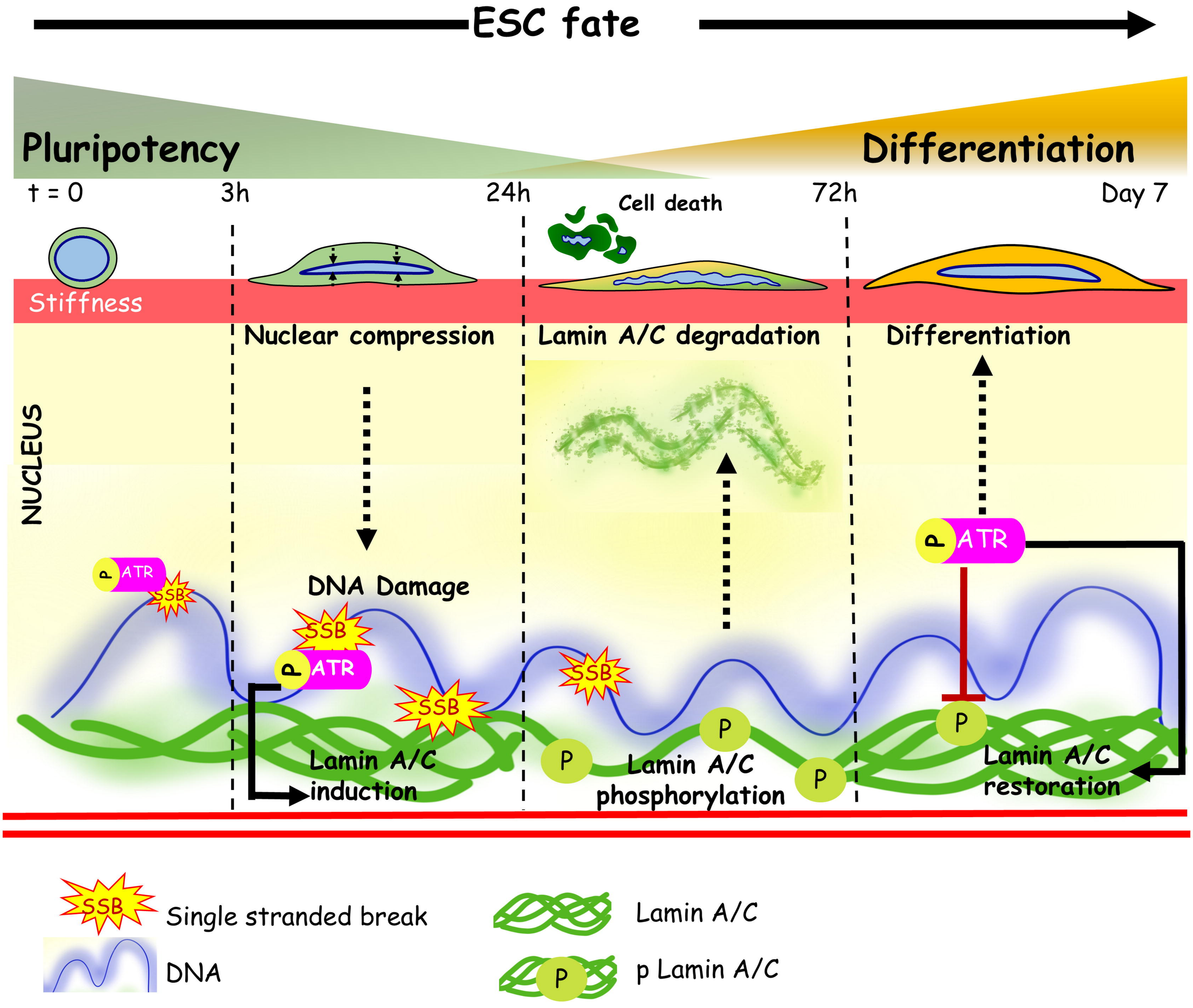
ESC fate
Pluripotency
Differentiation
t = 0
3h
24h
72h
Day 7
Cell death
Stiffness
Nuclear compression
Lamin A/C degradation
Differentiation
NUCLEUS
DNA Damage
ATR
SSB
Lamin A/C induction
Lamin A/C phosphorylation
Lamin A/C restoration
P
Single stranded break
DNA
Lamin A/C
p Lamin A/C